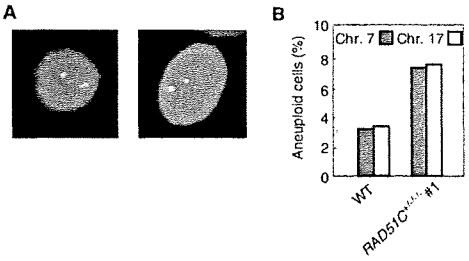

Figure 7. Increased aneuploidy. (A) FISH on Rad51C mutant cells using a probe for chromosome 7 (orange) and a probe for chromosome 17 (green). (B) Frequency of aneuploidy. For each chromosome-specific FISH, 500 cells were counted.

damage-response signal activated by Rad51C dysfunction causes chromosome instability by affecting centrosome integrity.

In contrast to previous studies using CL-V4B cells (11,12), the present study demonstrated that centrosome aberrations were induced by Rad51C dysfunction at both mitosis and interphase in two independent human cell lines. Since centrosome aberrations in interphase are likely to be generated at the S and G2 phases, such a difference may be explained by a mechanism that regulates centrosome integrity at these phases of the cell cycle. Given that the DNA damage response is involved in the maintenance of centrosome integrity, the absence of a protein involved in the signaling in response to unrepaired DNA damage may explain the lack of centrosome aberrations in interphase in CL-V4B cells.

A defect in the mismatch repair pathway has been shown to interfere with the DNA damage response (27). Since MLH1, a mismatch repair protein, is mutated in HCT116 cells, some phenotypes observed in the derivatives of this cell line are likely to be affected by a defect in mismatch repair. However, ATR-dependent centrosome aberrations in interphase were also observed in mismatch-proficient HT1080 cells, thus excluding this possibility.

The present results, together with those of previous studies (8–10,12), strengthen the role of Rad51 paralogs in the maintenance of centrosome integrity. However, it is unlikely that Rad51 paralogs directly regulate centrosome functions. There is no evidence to suggest that any member of the Rad51 paralog family localizes to the centrosome (7). We confirmed that Rad51C does not localize to the centrosome by exogenous expression of the *RAD51C* cDNA fused with the green fluorescent protein in Rad51C mutant cells (data not shown). Since Rad51C participates in the formation of two protein complexes consisting of five members of the Rad51 paralog family, these complexes are unlikely to localize to the centrosome.

Evidence that the DNA damage response plays a role in centrosome functions has been accumulating. ATM, ATR, ATRIP, Chk1 and Chk2 were shown to localize to the centrosome in HeLa cells (28). Supernumerary centrosomes in human lymphoblastoid cells exposed to ionizing radiation were cancelled by treatment with 2 mM caffeine or by the depletion of Chk1, suggesting that the ATM/ATR-Chk1 pathway may be involved in promoting centrosome amplification induced by DNA damage (16). The ATR-Chk1 pathway's role in regulating centrosome functions has been proposed from the identification of mutations in pericentrin, a centrosomal protein, in Seckel syndrome as well as in Majewski osteodysplastic primordial dwarfism type II (MOPD II) syndrome (29,30). These rare genetic disorders share dwarfism and microcephaly. Since ATR mutations are responsible for Seckel syndrome (31), the ATR-dependent DNA damage response signaling pathway might be associated with the pericentrin-dependent pathway. Although the exact role of ATR in centrosome functions remains to be elucidated, these results support the present finding that ATR is involved in increased supernumerary centrosomes. It is also noteworthy that caffeine treatment in Rad51C mutant cells did not reduce the frequency of centrosome aberrations to the wild-type levels, suggesting that an ATR-independent pathway may play a minor role in promoting centrosome aberrations in the mutant cells.

Defective homologous recombination causes prolonged replication fork arrest. Increased centrosome numbers that arise spontaneously in Rad51C mutant cells are likely to be attributable to prolonged arrest at replication forks or at the G2/M boundary. Furthermore, the present finding that ATR or Chk1 depletion reduced centrosome aberrations suggests that prolonged checkpoint arrest may cause supernumerary centrosomes. The previous finding that centrosome amplification induced by Rad51 deletion was caused during the prolonged G2 phase in an ATM-dependent manner supports this model (13). However, ATM is unlikely to be involved in the DNA damage response that increases centrosome numbers in Rad51C mutant cells. Although the interplay between ATM and ATR was shown to function in the DNA damage response (32,33), Rad51C dysfunction appears to activate the ATR-specific pathway. The DNA damage response signaling pathway activated by Rad51C dysfunction may be different from the pathway activated by depletion of Rad51. Rad51C may play a role in the DNA repair process that does not depend on Rad51. Rad51C or its associated proteins have been proposed to have a resolvase activity for Holliday junctions, suggesting that Rad51C may be involved in the late phase of homologous recombination (34). Thus, discrimination in the choice of the DNA damage response signal in their mutant cells may reflect functional differences between Rad51 and Rad51C in DSB repair through homologous recombination.

FUNDING

Japanese Society for Promoting Science (18310037 to K.M.); the Ministry of Education, Culture, Sports, Science and Technology (18012012 to K.M.); the Ministry of Health, Labor and Welfare of Japan (19140401 to K.M.); Hiroshima University 21st Century Center of Excellence Program (M.K. and T.Y.). Funding for open access charge: Japanese Society for Promoting Science.

Conflict of interest statement. None declared.

REFERENCES

1. West,S.C. (2003) Molecular views of recombination proteins and their control. *Nat. Rev. Mol. Cell Biol.*, **4**, 435–445.
2. Thacker,J. (2005) The RAD51 gene family, genetic instability and cancer. *Cancer Lett.*, **219**, 125–135.
3. Masson,J.-Y., Tarsounas,M.C., Stasiak,A.Z., Stasiak,A., Shah,R., McIlwraith,M.J., Benson,F.E. and West,S.C. (2001) Identification and purification of two distinct complexes containing the five RAD51 paralogs. *Genes Dev.*, **15**, 3296–3307.
4. Liu,N., Schild,D., Thelen,M.P. and Thompson,L.H. (2002) Involvement of Rad51C in two distinct protein complexes of Rad51 paralogs in human cells. *Nucleic Acids Res.*, **30**, 1009–1015.
5. Bettencourt-Dias,M. and Glover,D.M. (2007) Centrosome biogenesis and function: centrosomics brings new understanding. *Nat. Rev. Mol. Cell Biol.*, **8**, 451–463.
6. Nigg,E.A. (2006) Origins and consequences of centrosome aberrations in human cancers. *Int. J. Cancer*, **119**, 2717–2723.
7. Doxsey,S., Zimmerman,W. and Mikule,K. (2005) Centrosome control of the cell cycle. *Trends Cell Biol.*, **15**, 303–311.
8. Griffin,C.S., Simpson,P.J., Wilson,C.R. and Thacker,J. (2000) Mammalian recombination-repair genes XRCC2 and XRCC3 promote correct chromosome segregation. *Nat. Cell Biol.*, **2**, 757–761.
9. Smiraldo,P.G., Gruver,A.M., Osborn,J.C. and Pittman,D.L. (2005) Extensive chromosomal instability in Rad51d-deficient mouse cells. *Cancer Res.*, **65**, 2089–2096.
10. Date,O., Katsura,M., Ishida,M., Yoshihara,T., Kinomura,A., Sueda,T. and Miyagawa,K. (2006) Haploinsufficiency of RAD51B causes centrosome fragmentation and aneuploidy in human cells. *Cancer Res.*, **66**, 6018–6024.
11. Godthelp,B.C., Wiegant,W.W., van Duijn-Goedhart,A., Scharer,O.D., van Buul,P.P.W., Kanaar,R. and Zdzienicka,M.Z. (2002) Mammalian Rad51C contributes to DNA cross-link resistance, sister chromatid cohesion and genomic stability. *Nucleic Acids Res.*, **30**, 2172–2182.
12. Lindh,A.R., Schultz,N., Saleh-Gohari,N. and Helleday,T. (2007) RAD51C (RAD51L2) is involved in maintaining centrosome number in mitosis. *Cytogenet. Genome Res.*, **116**, 38–45.
13. Dodson,H., Bourke,E., Jeffers,L.J., Vagnarelli,P., Sonoda,E., Takeda,S., Earnshaw,W.C., Merdes,A. and Morrison,C. (2004) Centrosome amplification induced by DNA damage occurs during a prolonged G2 phase and involves ATM. *EMBO J.*, **23**, 3864–3873.
14. Daboussi,F., Thacker,J. and Lopez,B.S. (2005) Genetic interactions between RAD51 and its paralogues for centrosome fragmentation and ploidy control, independently of the sensitivity to genotoxic stresses. *Oncogene*, **24**, 3691–3696.
15. Pujana,M.A., Han,J.D., Starita,L.M., Stevens,K.N., Tewari,M., Ahn,J.S., Rennert,G., Moreno,V., Kirchhoff,T., Gold,B *et al.* (2007) Network modeling links breast cancer susceptibility and centrosome dysfunction. *Nat. Genet.*, **39**, 1338–1349.
16. Bourke,E., Dodson,H., Merdes,A., Cuffe,L., Zachos,G., Walker,M., Gillespie,D. and Morrison,C.G. (2007) DNA damage induces Chk1-dependent centrosome amplification. *EMBO Rep.*, **8**, 603–609.
17. Miyagawa,K., Tsuruga,T., Kinomura,A., Usui,K., Katsura,M., Tashiro,S., Mishima,H. and Tanaka,K. (2002) A role for RAD54B in homologous recombination in human cells. *EMBO J.*, **21**, 175–180.
18. Yoshihara,T., Ishida,M., Kinomura,A., Katsura,M., Tsuruga,T., Tashiro,S., Asahara,T. and Miaygawa,K. (2004) XRCC3 deficiency results in a defect in recombination and increased endoreduplication in human cells. *EMBO J.*, **23**, 670–680.
19. Yokoyama,H., Kurumizaka,H., Ikawa,S., Yokoyama,S. and Shibata,T. (2003) Holliday junction binding activity of the human Rad51B protein. *J. Biol. Chem.*, **278**, 2767–2772.
20. Hiyama,T., Katsura,M, Yoshihara,T., Ishida,M., Kinomura,A., Tonda,T., Asahara,T. and Miyagawa,K. (2006) Haploinsufficiency of the Mus81-Eme1 endonuclease activates the intra-S-phase and G_2/M checkpoints and promote rereplication in human cells. *Nucleic Acids Res.*, **34**, 880–892.
21. Bärlund,M., Monni,O., Kononen,J., Cornelison,R., Torhorst,J., Sauter,G., Kallioniemi,O-P. and Kallioniemi,A. (2000) Multiple genes at 17q23 undergo amplification and overexpression in breast cancer. *Cancer Res.*, **60**, 5340–5344.
22. Wu,G.-J., Sinclair,C.S., Paape,J., Ingle,J.N., Roche,P.C., James,C.D. and Couch,F.J. (2000) 17q23 amplifications in breast cancer involve the PAT1, RAD51C, PS6K, and SIGMA1B genes. *Cancer Res.*, **60**, 5371–5375.
23. Takata,M., Sasaki,M.S., Tachiiri,S., Fukushima,T., Sonoda,E., Schild,D., Thompson,L.H. and Takeda,S. (2001) Chromosome instability and defective recombinational repair in knockout mutants of the five Rad51 paralogs. *Mol. Cell Biol.*, **21**, 2858–2866.
24. Lio,Y.-C., Schild,D., Brenneman,M.A., Redpath,J.L. and Chen,D.J. (2004) Human Rad51C deficiency destabilizes XRCC3, impairs recombination, and radiosensitizes S/G2-phase cells. *J. Biol. Chem.*, **279**, 42313–42320.
25. Yu,Q., La Rose,J., Zhang,H., Takemura,H., Kohn,K.W. and Pommier,Y. (2002) UCN-01 inhibits p53 up-regulation and abrogates γ-radiation-induced G_2-M checkpoint independently of p53 by targeting both of the checkpoint kinases, Chk2 and Chk1. *Cancer Res.*, **62**, 5743–5748.
26. Löffler,H., Bochtler,T., Fritz,B., Tews,B., Ho,A.D., Lukas,J., Bartek,J. and Krämer,A. (2007) DNA damage-induced accumulation of centrosomal Chk1 contributes to its checkpoint function. *Cell Cycle*, **6**, 2541–2548.
27. Brown,K.D., Rathi,A., Kamath,R., Beardsley,D.I., Zhan,Q., Mannino,J.L. and Baskaran,R. (2003) The mismatch repair system is required for S-phase checkpoint activation. *Nat. Genet.*, **33**, 80–84.
28. Zhang,S., Hemmerich,P. and Grosse,F. (2007) Centrosomal localization of DNA damage checkpoint proteins. *J. Cell Biochem.*, **101**, 451–465.
29. Griffith,E., Walker,S., Martin,C.-A., Vagnarelli,P., Stiff,T., Vernay,B., Sanna,N.A., Saggar,A., Hamel,B., Earnshaw,W.C. *et al.* (2008) Mutations in pericentrin cause Seckel syndrome with defective ATR-dependent DNA damage signaling. *Nat. Genet.*, **40**, 232–236.
30. Rauch,A., Thiel,C.T., Schindler,D., Wick,U., Crow,Y.J., Ekici,A.B., van Essen,A.J., Goecke,T.O., Al-Gazali,L., Chrzanowska,K.H. *et al.* (2008) Mutations in the pericentrin (PCNT) gene cause primordial dwarfism. *Science*, **319**, 816–819.
31. O'Driscoll,M., Ruiz-Perez,V.L., Woods,C.G., Jeggo,P.A. and Goodship,J.A. (2003) A splicing mutation affecting expression of ataxia-telangiectasia and Rad3-related protein (ATR) results in Seckel syndrome. *Nat. Genet.*, **33**, 497–501.
32. Jazayeri,A., Falck,J., Lukas,C., Bartek,J., Smith,G.C.M., Lukas,J. and Jackson,S.P. (2006) ATM- and cell cycle-dependent regulation of ATR in response to DNA double-strand breaks. *Nat. Cell Biol.*, **8**, 37–45.
33. Stiff,T., Walker,S.A., Cerosaletti,K., Goodarzi,A.A., Petermann,E., Concannon,P., O'Driscoll,M. and Jeggo,P.A. (2006) ATR-dependent phosphorylation and activation of ATM in response to UV treatment or replication fork stalling. *EMBO J.*, **25**, 5775–5782.
34. Liu,Y., Masson,J.-Y., Shah,R., O'Regan,P. and West,S.C. (2004) RAD51C is required for Holliday junction processing in mammalian cells. *Science*, **303**, 243–246.

THE JOURNAL OF BIOLOGICAL CHEMISTRY VOL. 284, NO. 21, pp. 14326–14336, May 22, 2009

Recombination Activator Function of the Novel RAD51- and RAD51B-binding Protein, Human EVL*[S]

Received for publication, October 6, 2008, and in revised form, March 25, 2009 Published, JBC Papers in Press, March 26, 2009, DOI 10.1074/jbc.M807715200

Motoki Takaku[‡], Shinichi Machida[‡], Noriko Hosoya[§], Shugo Nakayama[‡], Yoshimasa Takizawa[‡], Isao Sakane[‡], Takehiko Shibata[¶], Kiyoshi Miyagawa[§], and Hitoshi Kurumizaka[‡1]

From the [‡]Laboratory of Structural Biology, Graduate School of Advanced Science and Engineering, and Consolidated Research Institute for Advanced Science and Medical Care, Waseda University, 2-2 Wakamatsu-cho, Shinjuku-ku, Tokyo 162-8480, the [§]Laboratory of Molecular Radiology, Center of Disease Biology and Integrative Medicine, Graduate School of Medicine, University of Tokyo, 7-3-1 Hongo, Bunkyo-ku, Tokyo 113-0033, and the [¶]RIKEN Advanced Science Institute, 2-1 Hirosawa, Wako-shi, Saitama 351-0198, Japan

The RAD51 protein is a central player in homologous recombinational repair. The RAD51B protein is one of five RAD51 paralogs that function in the homologous recombinational repair pathway in higher eukaryotes. In the present study, we found that the human EVL (Ena/Vasp-like) protein, which is suggested to be involved in actin-remodeling processes, unexpectedly binds to the RAD51 and RAD51B proteins and stimulates the RAD51-mediated homologous pairing and strand exchange. The EVL knockdown cells impaired RAD51 assembly onto damaged DNA after ionizing radiation or mitomycin C treatment. The EVL protein alone promotes single-stranded DNA annealing, and the recombination activities of the EVL protein are further enhanced by the RAD51B protein. The expression of the EVL protein is not ubiquitous, but it is significantly expressed in breast cancer-derived MCF7 cells. These results suggest that the EVL protein is a novel recombination factor that may be required for repairing specific DNA lesions, and that may cause tumor malignancy by its inappropriate expression.

Chromosomal DNA double strand breaks (DSBs)[2] are potential inducers of chromosomal aberrations and tumorigenesis, and they are accurately repaired by the homologous recombinational repair (HRR) pathway, without base substitutions, deletions, and insertions (1–3). In the HRR pathway (4, 5), single-stranded DNA (ssDNA) tails are produced at the DSB sites. The RAD51 protein, a eukaryotic homologue of the bacterial RecA protein, binds to the ssDNA tail and forms a helical nucleoprotein filament. The RAD51-ssDNA filament then binds to the intact double-stranded DNA (dsDNA) to form a three-component complex, containing ssDNA, dsDNA, and the RAD51 protein. In this three-component complex, the RAD51 protein promotes recombination reactions, such as homologous pairing and strand exchange (6–9).

The RAD51 protein requires auxiliary proteins to promote the homologous pairing and strand exchange reactions efficiently in cells (10–12). In humans, the RAD52, RAD54, and RAD54B proteins directly interact with the RAD51 protein (13–17) and stimulate the RAD51-mediated homologous pairing and/or strand exchange reactions *in vitro* (18–21). The human RAD51AP1 protein, which directly binds to the RAD51 protein (22), was also found to stimulate RAD51-mediated homologous pairing *in vitro* (23, 24). The BRCA2 protein contains ssDNA-binding, dsDNA-binding, and RAD51-binding motifs (25–33), and the *Ustilago maydis* BRCA2 ortholog, Brh2, reportedly stimulated RAD51-mediated strand exchange (34, 35). Most of these RAD51-interacting factors are known to be required for efficient RAD51 assembly onto DSB sites in cells treated with ionizing radiation (10–12).

The RAD51B (RAD51L1, Rec2) protein is a member of the RAD51 paralogs, which share about 20–30% amino acid sequence similarity with the RAD51 protein (36–38). *RAD51B*-deficient cells are hypersensitive to DSB-inducing agents, such as cisplatin, mitomycin C (MMC), and γ-rays, indicating that the RAD51B protein is involved in the HRR pathway (39–44). Genetic experiments revealed that *RAD51B*-deficient cells exhibited impaired RAD51 assembly onto DSB sites (39, 44), suggesting that the RAD51B protein functions in the early stage of the HRR pathway. Biochemical experiments also suggested that the RAD51B protein participates in the early to late stages of the HRR pathway (45–47).

In the present study, we found that the human EVL (Ena/Vasp-like) protein binds to the RAD51 and RAD51B proteins in a HeLa cell extract. The EVL protein is known to be involved in cytoplasmic actin remodeling (48) and is also overexpressed in breast cancer (49). Like the RAD51B knockdown cells, the EVL knockdown cells partially impaired RAD51 foci formation after DSB induction, suggesting that the EVL protein enhances RAD51 assembly onto DSB sites. The purified EVL protein preferentially bound to ssDNA and stimulated RAD51-mediated homologous pairing and strand exchange. The EVL protein also promoted the annealing of complementary strands. These recombination reactions that were stimulated or promoted by the EVL protein were further enhanced by the

* This work was supported in part by grants-in-aid from the Ministry of Education, Culture, Sports, Science, and Technology, Japan.
[S] The on-line version of this article (available at http://www.jbc.org) contains supplemental Figs. 1–3.
[1] To whom correspondence should be addressed. Tel.: 81-3-5369-7315; Fax: 81-3-5367-2820; E-mail: kurumizaka@waseda.jp.
[2] The abbreviations used are: DSB, double strand break; HRR, homologous recombinational repair; ssDNA, single-stranded DNA; dsDNA, double-stranded DNA; MMC, mitomycin C; NTA, nitrilotriacetic acid; HPLC, high performance liquid chromatography; SPR, surface plasmon resonance; DTT, dithiothreitol; AMPPNP, 5′-adenylyl-β,γ-imidodiphosphate; BSA, bovine serum albumin; siRNA, small interfering RNA.

RAD51B protein. These results strongly suggested that the EVL protein is a novel factor that activates RAD51-mediated recombination reactions, probably with the RAD51B protein. We anticipate that, in addition to its involvement in cytoplasmic actin dynamics, the EVL protein may be required in homologous recombination for repairing specific DNA lesions, and it may cause tumor malignancy by inappropriate recombination enhanced by EVL overexpression in certain types of tumor cells.

EXPERIMENTAL PROCEDURES

Purification of the Human EVL Protein—The human *EVL* gene was isolated from a human cDNA pool (purchased from Clontech) by polymerase chain reaction and was cloned in the pET-15b vector (Novagen). In this construct, the hexahistidine tag sequence was fused at the N-terminal end of the gene. The EVL protein was expressed in the *Escherichia coli* JM109(DE3) strain, which also carried an expression vector for the minor tRNAs (Codon(+)RIL; Stratagene). The cells producing the EVL protein were resuspended in buffer containing 20 mM potassium phosphate (pH 8.5), 700 mM NaCl, 5 mM 2-mercaptoethanol, 10 mM imidazole, and 10% glycerol and were disrupted by sonication. The cell debris was removed by centrifugation for 20 min at 30,000 × *g*, and the lysate was mixed gently by the batch method with Ni^{2+}-NTA-agarose beads (8 ml; Qiagen) at 4 °C for 1 h. The EVL-bound beads were washed with 80 ml of buffer containing 20 mM potassium phosphate (pH 8.5), 700 mM NaCl, 5 mM 2-mercaptoethanol, 30 mM imidazole, and 10% glycerol. The beads were then washed with 80 ml of buffer containing 20 mM potassium phosphate (pH 8.5), 700 mM NaCl, 5 mM 2-mercaptoethanol, 60 mM imidazole, and 10% glycerol and then were washed again with buffer containing 20 mM potassium phosphate (pH 8.5), 700 mM NaCl, 5 mM 2-mercaptoethanol, 30 mM imidazole, and 10% glycerol. The beads were then packed into an Econo-column (Bio-Rad) and were washed with 300 ml of buffer containing 20 mM potassium phosphate (pH 8.5), 100 mM NaCl, 5 mM 2-mercaptoethanol, 30 mM imidazole, and 10% glycerol. The His_6-tagged EVL protein was eluted with a 30-column volume linear gradient of 30–300 mM imidazole, in 20 mM potassium phosphate (pH 8.5), 100 mM NaCl, 5 mM 2-mercaptoethanol, and 10% glycerol. The fractions containing the His_6-tagged EVL protein were diluted with the same volume of buffer, containing 10 mM potassium phosphate (pH 8.5), 100 mM NaCl, 5 mM 2-mercaptoethanol, and 10% glycerol, and were mixed gently by the batch method with hydroxyapatite resin (10 ml; Bio-Rad) at 4 °C for 1 h. The resin was then washed with 80 ml of buffer, containing 20 mM potassium phosphate (pH 8.5), 100 mM NaCl, 5 mM 2-mercaptoethanol, and 10% glycerol, and was packed into an Econo-column (Bio-Rad). The resin was further washed with 300 ml of buffer, containing 20 mM potassium phosphate (pH 8.5), 225 mM NaCl, 5 mM 2-mercaptoethanol, and 10% glycerol, and then the His_6-tagged EVL protein was eluted with a 30-column volume linear gradient of 225–1000 mM NaCl and 10–300 mM potassium phosphate (pH 8.5). The His_6 tag was uncoupled from the EVL portion by a digestion with 5.5 units of thrombin protease (GE Healthcare) per mg of the His_6-tagged EVL protein, and then the protein was immediately dialyzed against buffer containing 20 mM potassium phosphate (pH 7.5), 200 mM NaCl, 5 mM 2-mercaptoethanol, and 10% glycerol at 4 °C. After uncoupling of the His_6 tag, the EVL protein was further purified by Superdex 200 gel filtration column (HiLoad 26/60 preparation grade; GE Healthcare) chromatography, followed by Mono S column chromatography. The peak fractions were diluted with the same volume of buffer, containing 20 mM potassium phosphate (pH 7.5), 5 mM 2-mercaptoethanol, and 10% glycerol, and were subjected to MonoS (GE Healthcare) column chromatography. The column was washed with 20 column volumes of buffer, containing 20 mM potassium phosphate (pH 7.5), 100 mM NaCl, 5 mM 2-mercaptoethanol, and 10% glycerol, and the EVL protein was eluted with a 12-column volume linear gradient of 100–600 mM NaCl. The purified EVL protein was dialyzed against buffer containing 20 mM HEPES-NaOH (pH 7.3), 100 mM NaCl, 5 mM 2-mercaptoethanol, and 30% glycerol and was stored at −80 °C. The concentration of the purified EVL protein was determined by the Bradford method, using bovine serum albumin (BSA) as the standard.

Purification of the Human RAD51, RAD51B, DMC1, and RPA Proteins—The human RAD51 protein (50), human RAD51B protein (47), human DMC1 protein (51), and human RPA protein (52) were purified by the methods described previously.

DNA Substrates—Single-stranded ϕX174 viral (+) strand DNA and double-stranded ϕX174 replicative form I DNA were purchased from New England Biolabs. The linear dsDNA was prepared from the ϕX174 replicative form I DNA by PstI digestion. In the D-loop formation assay, superhelical dsDNA (pB5Sarray DNA) was prepared by a method to prevent irreversible denaturation of the dsDNA substrate by alkaline treatment of the cells harboring the plasmid DNA. The cells were gently lysed using Sarkosyl, as described previously (15). The pB5Sarray DNA contained 11 repeats of a sea urchin 5 S rRNA gene (207-bp fragment) within the pBlueScript II SK(+) vector. For the ssDNA annealing assay, the following high performance liquid chromatography (HPLC)-purified oligonucleotides were purchased from Nihon Gene Research Laboratory: 5′-GTC CCA GGC CAT TAC AGA TCA ATC CTG AGC ATG TTT ACC AAG CGC ATT G-3′ and 5′-CAA TGC GCT TGG TAA ACA TGC TCA GGA TTG ATC TGT AAT GGC CTG GGA C-3′. For the ssDNA substrate used in the D-loop assay, the following HPLC-purified oligonucleotide was purchased: 50-mer, 5′-GGA ATT CGG TAT TCC CAG GCG GTC TCC CAT CCA AGT ACT AAC CGA GCC CT-3′. The DNA sequences used in the strand exchange assay with the oligonucleotides are as follows: 63-mer, 5′-TCC TTT TGA TAA GAG GTC ATT TTT GCG GAT GGC TTA GAG CTT AAT TGC TGA ATC TGG TGC TGT-3′; 32-mer top strand, 5′-CCA TCC GCA AAA ATG ACC TCT TAT CAA AAG GA-3′; 32-mer bottom strand, 5′-TCC TTT TGA TAA GAG GTC ATT TTT GCG GAT GG-3′. The 5′-ends of the oligonucleotide (32-mer bottom strand) were labeled with T4 polynucleotide kinase (New England Biolabs) in the presence of [γ-^{32}P]ATP at 37 °C for 30 min. All DNA concentrations are expressed in moles of nucleotides.

Pulldown Assays with EVL-conjugated Beads—The EVL protein was covalently conjugated to Affi-Gel 10 beads (100 μl;

Bio-Rad), according to the manufacturer's instructions. To block the remaining active ester sites, ethanolamine (pH 8.0) was added to a final concentration of 100 mM, and the resin was incubated at 4 °C overnight. The unbound proteins were removed by washing the Affi-Gel 10-EVL beads three times with 500 μl of binding buffer, which contained 20 mM HEPES-NaOH (pH 7.3), 100 mM NaCl, 5 mM 2-mercaptoethanol, 30% glycerol, and 0.05% Triton X-100. After washing the resin, the Affi-Gel 10-protein matrices were adjusted to 50% slurries and were stored at 4 °C.

For the RAD51B-binding and RAD51-binding assays, the EVL beads were incubated with a HeLa whole cell extract (2 mg of protein), and the beads were washed three times with 200 μl of washing buffer, containing 50 mM potassium phosphate (pH 7.5), 100 mM NaCl, 5 mM EDTA, 0.5% Nonidet P-40, and protease inhibitor mixture (Nacalai Tesque). The proteins that copelleted with the EVL beads were separated into two portions for the RAD51 and RAD51B analyses and were fractionated by 12% SDS-PAGE. The RAD51 and RAD51B proteins were detected with the RAD51-specific and RAD51B-specific rabbit polyclonal antibodies, respectively.

Pulldown Assays with the Ni^{2+}-NTA-Agarose Beads—The His_6-tagged EVL protein (0.45 μM) was prepared and was mixed with the RAD51 or RAD51B protein (2 μM) in 20 mM HEPES buffer (pH 7.3), containing 95 mM NaCl, 0.1 mM EDTA, 0.045% Triton X-100, 1.8 mM ammonium sulfate, 2 mM 2-mercaptoethanol, 4.5 mM imidazole, and 29% glycerol. After a 30-min incubation at room temperature, 1.5 μl of the Ni^{2+}-NTA-agarose beads were added to the reaction mixture, and the RAD51 or RAD51B protein bound to the His_6-tagged EVL protein was captured by the beads. The beads were washed two times with 100 μl of washing buffer, containing 20 mM HEPES-NaOH (pH 7.3), 90 mM NaCl, 0.1 mM EDTA, 0.05% Triton X-100, 2 mM ammonium sulfate, 2 mM 2-mercaptoethanol, 5 mM imidazole, and 30% glycerol. The proteins that copelleted with the Ni^{2+}-NTA beads were eluted with a buffer, containing 14 mM HEPES-NaOH (pH 7.3), 100 mM NaCl, 3.5 mM 2-mercaptoethanol, 300 mM imidazole, and 21% glycerol. The eluted fractions were analyzed by 12% SDS-PAGE with Coomassie Brilliant Blue staining.

Surface Plasmon Resonance Analysis—The surface plasmon resonance (SPR) signals were measured with a Biacore J instrument (GE Healthcare). Flow cells were maintained at 25 °C during the measurement, and the instrument was operated at the mid-flow rate (~30 μl/min). The EVL protein was conjugated to the activated surface of CM5 sensor chips (GE Healthcare), using the standard amine coupling conditions recommended by the manufacturer. The level of the conjugated EVL protein was 3,860 resonance units. Reference SPR signals of the flow cell containing a sensor chip without the EVL protein were subtracted from those of the SPR signals of the flow cell containing the EVL-conjugated sensor chip. The running buffer was 20 mM HEPES-NaOH (pH 7.3), 150 mM NaCl, 2 mM ammonium sulfate, 5% glycerol, and 0.05% Triton X-100. Before each binding assay, the sensor chip was regenerated by a 1-min wash with 10 mM NaOH and two 1-min washes with 20 mM citrate buffer (pH 2.65), followed by a 25-min wash with the running buffer. For each binding assay, 1 μM analyte solution (*i.e.* the RAD51 protein, the RAD51B protein, the DMC1 protein, or the BSA solution) was injected for 5 min.

Assays for DNA Binding—The φX174 circular ssDNA (20 μM) or the linearized φX174 dsDNA (20 μM) was mixed with the EVL protein in 10 μl of a standard reaction solution, containing 36 mM HEPES-NaOH buffer (pH 7.5) with 1 mM dithiothreitol, 4 mM 2-mercaptoethanol, 80 mM NaCl, 1 mM $MgCl_2$, 24% glycerol, and 0.1 mg/ml BSA. The reaction mixtures were incubated at 37 °C for 15 min and were then analyzed by 0.8% agarose gel electrophoresis in 1× TAE buffer (40 mM Tris acetate and 1 mM EDTA) at 3.3 V/cm for 2 h. The bands were visualized by ethidium bromide staining.

The D-loop Formation Assay—The indicated amount of the EVL protein was incubated in the presence or absence of the RAD51 protein (0.1 μM) at 37 °C for 5 min in the reaction buffer, containing 26 mM HEPES-NaOH (pH 7.5), 40 mM NaCl, 0.02 mM EDTA, 0.9 mM 2-mercaptoethanol, 5% glycerol, 1 mM $MgCl_2$, 1 mM DTT, 2 mM AMPPNP, and 0.1 mg/ml BSA. After this incubation, the ^{32}P-labeled 50-mer oligonucleotide (1 μM) was added, and the samples were further incubated at 37 °C for 5 min. The reactions were then initiated by the addition of the pB5Sarray superhelical dsDNA (60 μM) along with 9 mM $MgCl_2$ and were continued at 37 °C for 30 min. The reactions were stopped by the addition of 0.2% SDS and 1.5 mg/ml proteinase K and were further incubated at 37 °C for 15 min. After adding 6-fold loading dye, the deproteinized reaction products were separated by 1% agarose gel electrophoresis in 1× TAE buffer at 3.3 V/cm for 2.5 h. The gels were dried, exposed to an imaging plate, and visualized using an FLA-7000 imaging analyzer (Fujifilm).

Assays for Homologous Pairing with Oligonucleotides—For the homologous pairing assay with oligonucleotides, the RAD51 protein and the indicated amounts of the EVL protein were incubated with a 63-mer ssDNA (15 μM) in 10 μl of standard reaction buffer, containing 28 mM HEPES-NaOH (pH 7.5), 50 mM NaCl, 1 mM ATP, 1 mM DTT, 0.1 mg/ml BSA, 1 mM $MgCl_2$, 1 mM $CaCl_2$, 0.02 mM EDTA, 1.4 mM 2-mercaptoethanol, 20 mM creatine phosphate, 75 μg/ml creatine kinase, and 8% glycerol at 37 °C for 10 min. The strand exchange reaction was initiated by the addition of the 32-mer dsDNA (1.5 μM), which shared sequence homology with the 63-mer ssDNA. After a 30-min incubation at 37 °C, the reaction was stopped by the addition of 0.2% SDS and 1.5 mg/ml proteinase K. The reaction mixtures were further incubated for 10 min at 37 °C. After 6-fold loading dye was added, the reaction mixtures were subjected to 15% polyacrylamide gel electrophoresis in 0.5× TBE buffer (45 mM Tris, 45 mM boric acid, and 1 mM EDTA) at 10 V/cm for 5 h. The gels were dried, exposed to an imaging plate, and visualized using an FLA-7000 imaging analyzer.

Assay for Strand Exchange—The RAD51 protein (1 μM) and RPA (1 μM) were incubated with the indicated amounts of the EVL protein and/or the RAD51B protein at 30 °C for 10 min, in 8 μl of reaction buffer, containing 28 mM HEPES-NaOH (pH 7.5), 2.5 mM Tris-HCl (pH 7.5), 49 mM NaCl, 5 mM KCl, 0.03 mM EDTA, 1.1 mM 2-mercaptoethanol, 9% glycerol, 0.2 mM ammonium sulfate, 0.005% Triton X-100, 1 mM $MgCl_2$, 1 mM $CaCl_2$, 1.1 mM DTT, 1 mM ATP, 0.1 mg/ml BSA, 20 mM creatine phosphate, and 75 μg/ml creatine kinase. After this incubation,

ϕX174 circular ssDNA (20 μM) was added, and the samples were further incubated at 30 °C for 10 min. The reactions were then initiated by the addition of ϕX174 linear dsDNA (20 μM) and were continued at 30 °C for 60 min. The reactions were stopped by the addition of 0.2% SDS and 1.5 mg/ml proteinase K (Roche Applied Science) and were further incubated for 20 min. After adding 6-fold loading dye, the deproteinized reaction products were separated by 1% agarose gel electrophoresis in 1 × TAE buffer at 3.3 V/cm for 4 h. The products were visualized by SYBR Gold (Invitrogen) staining.

ssDNA Annealing Assay—The ssDNA oligonucleotide 49-mer (0.2 μM) was incubated with the indicated amounts of the EVL protein at 30 °C for 5 min in 9 μl of reaction buffer, containing 28 mM HEPES-NaOH (pH 7.5), 50 mM NaCl, 2 mM 2-mercaptoethanol, 12% glycerol, 0.1 mM $MgCl_2$, 1 mM DTT, and 0.1 mg/ml BSA. For the experiment with the RAD51B protein, the EVL protein was preincubated with the indicated amounts of the RAD51B protein at 30 °C for 10 min, in 8 μl of reaction buffer, containing 28 mM HEPES-NaOH (pH 7.5), 38 mM NaCl, 1.4 mM 2-mercaptoethanol, 12% glycerol, 0.4 mM ammonium sulfate, 0.01% Triton X-100, 1 mM $MgCl_2$, 1 mM DTT, 1 mM ATP, and 0.1 mg/ml BSA, before the addition of the ssDNA oligonucleotide. The reactions were initiated by the addition of 0.2 μM antisense ^{32}P-labeled 49-mer oligonucleotide. At the times indicated, the reactions were quenched with an excess of the unlabeled 49-mer oligonucleotide. The DNA substrates and products were deproteinized by 0.2% SDS and 1.5 mg/ml proteinase K at 30 °C for 10 min. The products were fractionated by 10% PAGE in 0.5× TBE. The gels were dried, exposed to an imaging plate, and visualized using an FLA-7000 imaging analyzer.

EVL and RAD51B Knockdown Experiments—Rabbit polyclonal antibodies for the EVL and RAD51B proteins were obtained with the purified recombinant EVL and RAD51B proteins as antigens. The RAD51 antibody was purchased from Calbiochem (anti-RAD51 Ab-1 rabbit polyclonal antibody), and the Cdk2 antibody was purchased from Santa Cruz Biotechnology (Anti-Cdk2 M2 rabbit polyclonal antibody). The siRNA duplexes (Stealth™ RNAi) were designed by the BLOCK-iT™ RNAi Designer (Invitrogen) and were purchased from Invitrogen. The siRNA sequences of EVL and RAD51B are as follows: 5′-CCAGUAAGAAAUGGGUACCAAUCAA-3′ (for EVL) and 5′-GAGGUGUCCAUGAACUUCUAU-GUAU-3′ (for RAD51B). The sequence of the control siRNA is 5′-CCAAGAAGUAAAUGGAACCUUGCAA-3′, in which the EVL siRNA sequence was shuffled. The cells were seeded in a 6-well plate. A 15-μl aliquot of siRNA (20 μM) was diluted with 185 μl of serum-free Dulbecco's modified Eagle's medium. In a separate tube, 2 μl of Dharma*FECT* 4 Transfection Reagent (Dharmacon) were diluted with 198 μl of serum-free Dulbecco's modified Eagle's medium, and the mixture was incubated at room temperature for 5 min. The diluted Dharma*FECT* 4 was combined with the diluted siRNA duplex, and the mixture was incubated at room temperature for 20 min. A 2-ml aliquot of Dulbecco's modified Eagle's medium was then added to the Dharma*FECT* 4-siRNA complex. This mixture was applied to the cells, which were then incubated at 37 °C for 48 h.

Western Blotting—The cells were harvested and were resuspended in lysis buffer, containing 50 mM Tris-HCl (pH 7.5), 100 mM NaCl, 5 mM EDTA, 0.5% Nonidet P-40, 1.7 μg/ml aprotinin, 50 nM cantharidin, 1 mM phenylmethylsulfonyl fluoride, and 10 nM microcystine. After a 30-min incubation on ice, the cell lysates were sonicated and were centrifuged at 20,000 × *g* for 5 min at 4 °C. The lysates (30 μg of protein/lane) were separated by 12% SDS-PAGE, and the proteins were transferred to a nitrocellulose membrane. The membrane was probed with anti-EVL rabbit polyclonal antibody, anti-RAD51B rabbit polyclonal antibody, or anti-Cdk2 rabbit polyclonal antibody and was developed using a horseradish peroxidase-conjugated anti-rabbit IgG antibody and the ECL Western blotting detection reagent (GE Healthcare).

Immunostaining—MCF7 cells were grown on glass coverslips and were either nontreated or irradiated with 8 or 20 grays, using the ^{137}Cs source in the Facilities for Biological Research, Department of Nuclear Engineering and Management, Graduate School of Engineering, University of Tokyo. At 2 h after irradiation, the cells were fixed in 4% paraformaldehyde for 10 min, washed with PBS, and permeabilized with 0.5% Triton X-100 and 0.1% SDS in PBS for 5 min. The coverslips were incubated for 1 h at 37 °C with an anti-RAD51 antibody diluted with blocking buffer (1% BSA in PBS) and were then washed again. The RAD51 foci were visualized by an incubation with a fluorescein isothiocyanate-conjugated secondary antibody diluted in blocking buffer for 30 min at 37 °C. The nuclei of the cells were stained with 4′,6′-diamidino-2-phenylindole.

For MMC treatment, the cells were incubated in medium containing 0.8 μg/ml MMC (KYOWA) for 1 h at 37 °C. The cells were then washed with PBS, incubated for 24 h at 37 °C, and immunostained as described above.

Sensitivity to MMC—MCF7 cells were treated with MMC in suspension for 1 h and were washed three times with PBS. The cells were then plated at a density of 2 × 10^3 cells/60-mm dish. After 12 days of culture, colonies were counted.

RESULTS

The EVL Protein Is Involved in RAD51 Assembly—To identify novel HRR factors, we screened a human cDNA library by the two-hybrid method, with the human RAD51 protein and/or the RAD51 paralogs as bait. We obtained 73 positive clones as putative RAD51B-interacting proteins and found that 30 clones among them contained *EVL* gene fragments. Six clones encoding the RAD51C protein, which is a known RAD51B-interacting protein, were also found among these positive clones, suggesting that the screening was properly performed.

Since RAD51B is known to be required for the RAD51 assembly onto DSB sites after exposure to ionizing radiation, we then tested whether the EVL protein functions in RAD51 assembly *in vivo*. To do so, we performed RNA interference experiments. A treatment with a short interfering RNA (siRNA) designed to target the EVL mRNA caused about a 90% reduction in the EVL level in MCF7 cells, as compared with the cells treated with a control siRNA (Fig. 1*A*). The siRNA designed to target the RAD51B mRNA caused about an 80% reduction in the RAD51B level, without influencing the EVL level (Fig. 1*A*).

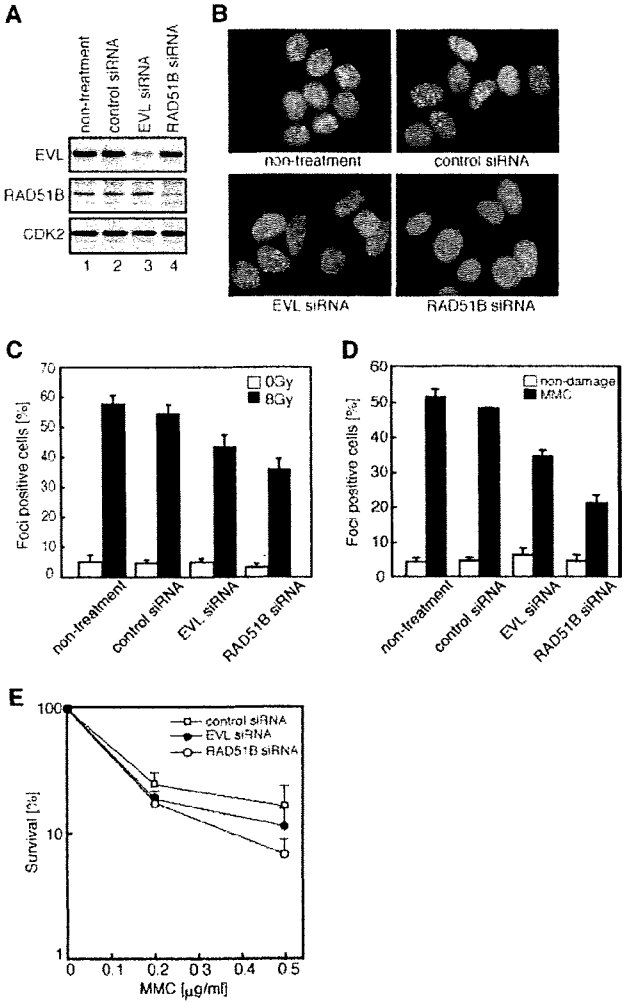

FIGURE 1. **Analyses of the EVL and RAD51B knockdown cells.** *A*, the EVL, RAD51B, and CDK2 proteins in the siRNA-treated MCF7 cells. The *top, middle,* and *bottom panels* indicate the expression levels of the EVL, RAD51B, and CDK2 proteins, respectively. The proteins were detected by Western blotting. *Lanes 1* and *2*, control experiments without siRNA and with a control siRNA, respectively. *Lanes 3* and *4*, experiments with EVL siRNA and RAD51B siRNA, respectively. *B*, RAD51 foci formation. The MCF7 cells were treated with γ-ray irradiation (8 grays). The cells without treatment, with a control siRNA treatment, with an EVL siRNA treatment, or with a RAD51B siRNA treatment are presented. *C*, graphic representation of the RAD51 foci formation after γ-ray irradiation (8 grays). The cells containing more than 10 RAD51 foci were scored as positive and were plotted. The averages of three independent experiments are plotted with S.D. values. *D*, graphic representation of the RAD51 foci formation after MMC treatment. The cells containing more than 10 RAD51 foci were scored as positive and were plotted. The averages of three independent experiments are plotted with S.D. values. *E*, sensitivity to MMC. *Open squares, closed circles,* and *open circles,* experiments with a control siRNA, EVL siRNA, and RAD51B siRNA, respectively. The averages of three independent experiments are plotted with S.D. values.

The cells containing more than ten RAD51 foci after ionizing radiation treatment were scored as positive, because many cells containing fewer than 10 RAD51 foci were observed, even in the absence of DNA damage. The EVL knockdown MCF7 cells exhibited a clear reduction in RAD51 foci formation (Fig. 1, *B* and *C*, and supplemental Fig. 1). Consistent with previous studies (39, 44), the RAD51B knockdown MCF7 cells exhibited a comparable reduction in RAD51 foci formation on the DSB

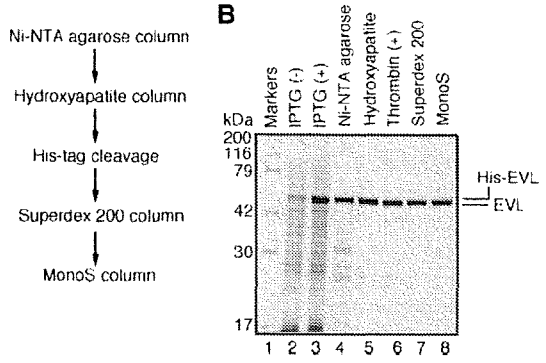

FIGURE 2. **Purification of the human EVL protein.** *A*, schematic representation of the purification steps for the Evl protein. *B*, proteins from each purification step were analyzed by 12% SDS-PAGE with Coomassie Brilliant Blue staining. *Lane 1*, molecular mass markers; *lanes 2* and *3*, whole cell lysates before and after induction with isopropyl-1-thio-β-D-galactopyranoside (*IPTG*), respectively. *Lanes 4–8*, samples from the peak Ni^{2+}-NTA-agarose (Invitrogen) fraction, the peak hydroxyapatite (Bio-Rad) fraction, the fraction after the removal of the hexahistidine tag, the peak Superdex 200 fraction (GE Healthcare), and the peak MonoS fraction (GE Healthcare), respectively.

sites after ionizing radiation (Fig. 1, *B* and *C*). Reduced RAD51 foci formation was also observed in the EVL knockdown cells after treatment with an interstrand cross-linking agent, MMC (Fig. 1*D*). These results suggested that, like the RAD51B protein, the EVL protein functions in RAD51 assembly on DSB sites in the HRR pathway.

On the other hand, the EVL knockdown cells did not exhibit significant increase in sensitivity to MMC (Fig. 1*E*). The weak MMC sensitivity in the EVL knockdown cells, as compared with that in the RAD51B knockdown cells, may be explained by the presence of EVL paralogs, such as the MENA and VASP proteins, which may complement the functions of the EVL protein.

Interaction of the EVL Protein with the RAD51 and RAD51B Proteins—The human EVL protein was purified as a recombinant protein by a five-step procedure (Fig. 2*A*). In this procedure, the His_6 tag was uncoupled with thrombin protease from the EVL portion, which then migrated slightly faster than the His_6-tagged EVL protein upon SDS-polyacrylamide gel electrophoresis (Fig. 2*B*, *lane 6*).

We then tested whether the EVL protein binds to the RAD51 protein, because the EVL knockdown cells exhibited a reduction in RAD51 foci formation (Fig. 1, *B* and *C*). To do so, we prepared Affi-Gel 10 beads chemically conjugated with the EVL protein and performed pulldown assays with HeLa cell extracts. As shown in Fig. 3*A* (*lane 2*), the endogenous RAD51 protein in the HeLa cell extract was detected in the EVL-bound fraction over the background level. Like the RAD51 protein, the endogenous RAD51B protein in the HeLa cell extract was also detected in the EVL-bound fraction (Fig. 3*B*, *lane 2*). These results suggested that the EVL protein binds to the RAD51 and RAD51B proteins.

To verify the EVL binding to the RAD51 and RAD51B proteins, we performed SPR analyses. The RAD51 protein interacted with the EVL-conjugated sensor chip (Fig. 3*C*). The RAD51B protein also significantly interacted with the EVL protein (Fig. 3*D*). In contrast, the DMC1 protein, which shares about 50% amino acid identity with the RAD51 protein, exhib-

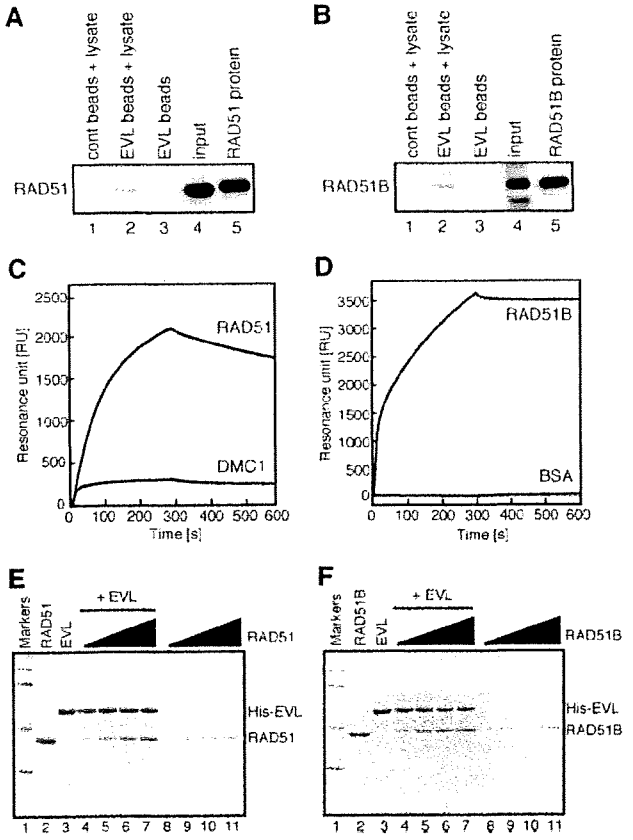

FIGURE 3. **The EVL protein binds to the RAD51 and RAD51B proteins.** *A* and *B*, pulldown assay. Affi-Gel 10 beads chemically conjugated with the EVL protein were incubated with a HeLa whole cell extract. Proteins bound to the EVL beads were separated by SDS-PAGE and were analyzed by Western blotting. *A*, the endogenous RAD51 protein was probed with an anti-RAD51 polyclonal antibody. *Lanes 1* and *2*, experiments with the control Affi-Gel 10 beads and the EVL beads, respectively, in the presence of the HeLa cell lysate. *Lane 3*, a control experiment with the EVL beads in the absence of the HeLa cell lysate. The input HeLa cell lysate (10 μg of protein) and the purified RAD51 (2 ng) protein were applied in *lanes 4* and *5*, respectively. *B*, the endogenous RAD51B protein was probed with an anti-RAD51B polyclonal antibody. *Lanes 1* and *2*, experiments with the control Affi-Gel 10 beads and the EVL beads, respectively, in the presence of the HeLa cell lysate. *Lane 3*, a control experiment with the EVL beads in the absence of the HeLa cell lysate. The input HeLa cell lysate (10 μg) and the purified RAD51B protein (2 ng) were applied in *lanes 4* and *5*, respectively. *C*, surface plasmon resonance analyses of the EVL-RAD51 and EVL-DMC1 interactions. Sensorgrams for RAD51 and DMC1 binding to the immobilized EVL protein are presented. The RAD51 and DMC1 concentrations were 1 μM. *D*, surface plasmon resonance analysis of the EVL-RAD51B interaction. Sensorgrams for RAD51B and BSA binding to the immobilized EVL protein are presented. The RAD51B and BSA concentrations were 1 μM. *E* and *F*, the Ni^{2+}-NTA-agarose pulldown assay with the His_6-tagged EVL and RAD51 (*E*) or RAD51B (*F*) proteins. *Lane 1*, molecular mass markers (200, 116, 79, 42, and 30 kDa). *Lanes 2* and *3*, RAD51 (*E*) or RAD51B (*F*) and the His_6-tagged EVL proteins. *Lanes 4–7* and *lanes 8–11*, experiments in the presence and absence of the His_6-tagged EVL, respectively. The concentration of the His_6-tagged EVL protein was 0.45 μM. The RAD51 or RAD51B concentrations were 0.5 μM (*lanes 4* and *8*), 1 μM (*lanes 5* and *9*), 1.5 μM (*lanes 6* and *10*), and 2 μM (*lanes 7* and *11*).

ited little binding to the EVL protein (Fig. 3*C*). These results indicated that the EVL protein specifically binds to the RAD51 and RAD51B proteins.

We finally confirmed the EVL binding to the RAD51 and RAD51B proteins by the Ni^{2+}-NTA-agarose pulldown assay. In this assay, the His_6-tagged EVL protein was used as the bait

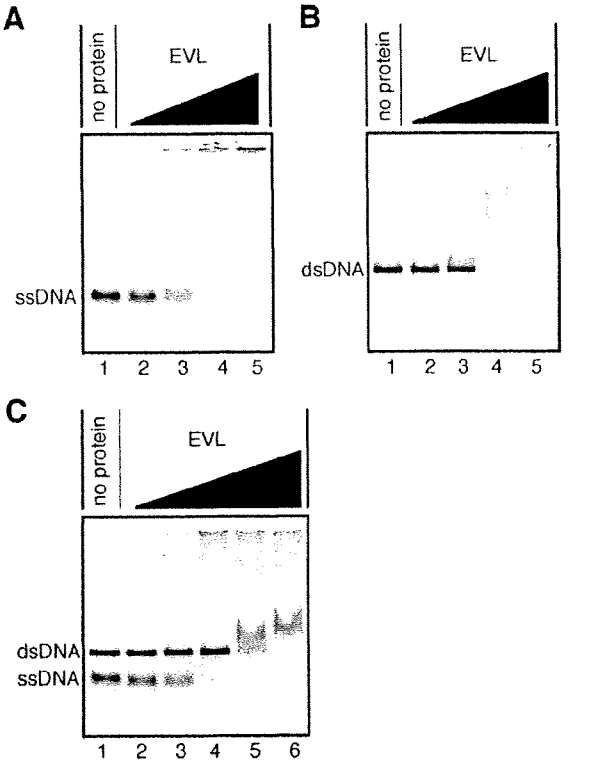

FIGURE 4. **DNA binding activities of the EVL protein.** ϕX174 ssDNA (20 μM) and/or ϕX174 linear dsDNA (20 μM) were each incubated with the EVL protein at 37 °C for 15 min. The samples were then separated by 0.8% agarose gel electrophoresis in TAE buffer and were visualized by ethidium bromide staining. *A*, ssDNA binding. *Lane 1*, a negative control experiment without the EVL protein. The EVL concentrations were 0.1 μM (*lane 2*), 0.2 μM (*lane 3*), 0.4 μM (*lane 4*), and 0.8 μM (*lane 5*). *B*, dsDNA binding. *Lane 1*, a negative control experiment without the EVL protein. The EVL concentrations were 0.1 μM (*lane 2*), 0.2 μM (*lane 3*), 0.4 μM (*lane 4*), and 0.8 μM (*lane 5*). *C*, competitive binding to ssDNA and dsDNA. *Lane 1*, a negative control experiment without the EVL protein. The EVL concentrations were 0.1 μM (*lane 2*), 0.2 μM (*lane 3*), 0.4 μM (*lane 4*), 0.8 μM (*lane 5*), and 1.2 μM (*lane 6*).

protein, since the EVL protein covalently conjugated to the Affi-gel beads did not enter the polyacrylamide gel. Consistently, the purified RAD51 and RAD51B proteins bound to the His_6-tagged EVL protein were captured by the Ni^{2+}-NTA beads in a concentration-dependent manner (Fig. 3, *E* and *F*). In the presence of excess amounts of the RAD51 and RAD51B proteins, the EVL:RAD51 and EVL:RAD51B ratios detected in the gel were 2.4:1 and 1.4:1, respectively (Fig. 3, *C* and *D*, *lane 7*). Therefore, we conclude that the EVL protein directly interacts with the RAD51 and RAD51B proteins.

The EVL Protein Stimulates RAD51-mediated Homologous Pairing—As shown in Fig. 4, *A* and *B*, the EVL protein bound to both ssDNA and dsDNA. A competitive DNA-binding assay revealed that the EVL protein preferentially bound to ssDNA rather than dsDNA (Fig. 4*C*). To study the EVL activity in the recombination reaction, we tested whether the EVL protein affects the RAD51-mediated homologous pairing. To do so, we performed the D-loop formation assay (Fig. 5*A*). The superhelical dsDNA used in this assay was prepared by a method without alkali treatment to avoid denaturation of the double helix of the dsDNA (15). As shown in Fig. 5, *B* (*lanes 2–4*) and *C*, the EVL

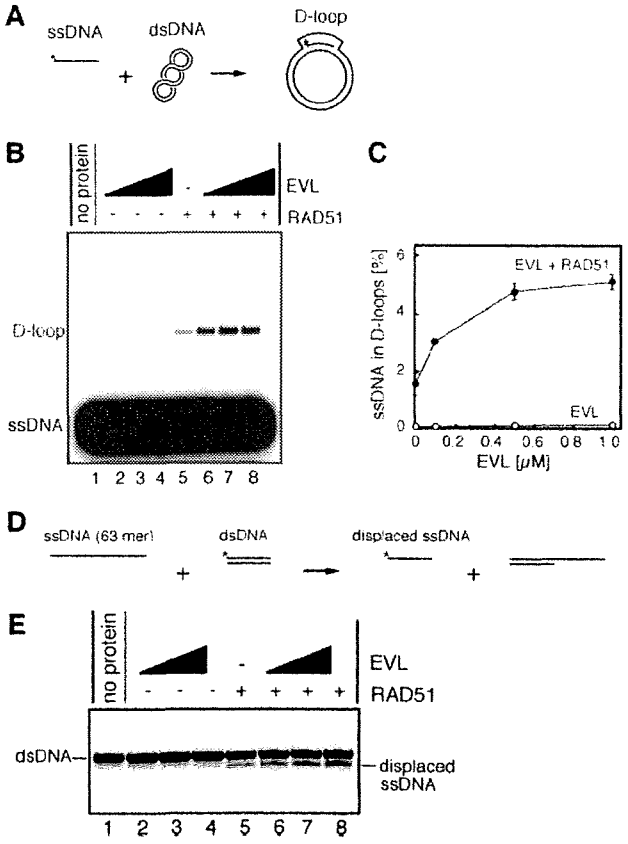

FIGURE 5. **The EVL protein stimulates the RAD51-mediated homologous pairing.** *A*, a schematic representation of the D-loop formation assay. *Asterisks* indicate the ^{32}P-labeled end of the 50-mer ssDNA. *B*, the D-loop formation assay. The reactions were conducted without the RAD51 protein (*lanes 1–4*) or with the RAD51 protein (0.1 μM) (*lanes 5–8*) in the presence of increasing amounts of the EVL protein. The EVL concentrations were 0 μM (*lanes 1* and *5*), 0.1 μM (*lanes 2* and *6*), 0.5 μM (*lanes 3* and *7*), and 1 μM (*lanes 4* and *8*). *C*, graphic representation of the experiments shown in *B*. *Closed* and *open circles*, experiments with and without the RAD51 protein, respectively. *D*, a schematic representation of the homologous pairing assay with oligonucleotides. The *asterisks* indicate the ^{32}P-labeled end of the 32-mer DNA strand. *E*, the homologous pairing assay. The reactions were conducted without the RAD51 protein (*lanes 1–4*) or with the RAD51 protein (1 μM) (*lanes 5–8*) in the presence of increasing amounts of the EVL protein. The EVL concentrations were 0 μM (*lanes 1* and *5*), 0.5 μM (*lanes 2* and *6*), 1 μM (*lanes 3* and *7*), and 2 μM (*lanes 4* and *8*).

protein alone did not promote D-loop formation. However, intriguingly, the amount of D-loops formed by the RAD51 protein synergistically increased, in an EVL concentration-dependent manner (Fig. 5, *B* (*lanes 5–8*) and *C*). Therefore, the EVL protein may have an activator function in homologous pairing by the RAD51 protein.

To confirm this EVL-mediated activation of homologous pairing, we performed the homologous pairing assay with short oligonucleotides (Fig. 5*D*). In this assay, a 63-mer ssDNA and a homologous 32-mer dsDNA were used as substrates. In the reaction, the ^{32}P-labeled 32-mer strand, which contains a sequence identical to that of the 63-mer ssDNA, is displaced from the dsDNA, as a consequence of the homologous pairing and subsequent strand exchange reactions by RAD51. As shown in Fig. 5*E* (*lanes 5–8*), the EVL protein enhanced the RAD51-mediated homologous pairing between the 63-mer ssDNA and the homologous 32-mer dsDNA. The displaced ^{32}P-labeled 32-mer product was not detected when the RAD51 protein was omitted from the reaction mixture (Fig. 5*E*, *lanes 2–4*), suggesting that the EVL protein alone did not promote homologous pairing. These results obtained from two independent homologous pairing assays are perfectly consistent; therefore, we conclude that the EVL protein stimulates the RAD51-mediated homologous pairing *in vitro*.

The EVL Protein Stimulates RAD51-mediated Strand Exchange—After homologous pairing, the RAD51 protein promotes a long tract of strand exchange, probably for the fine matching of homologous sequences. We next tested whether the EVL protein affects the RAD51-mediated strand exchange with long DNA substrates. In this assay, φX174 phage circular ssDNA (5,386 bases) and linearized φX174 dsDNA (5,386 base pairs) were used as DNA substrates (Fig. 6*A*). RPA is required for the efficient promotion of the strand exchange reaction by the RAD51 protein, but this RPA-dependent stimulation of strand exchange was not significant when the ssDNA was pre-incubated with RPA before the RAD51-ssDNA binding. This suppressive effect of RPA is considered to be overcome by the RAD51-binding proteins (11).

We then conducted the strand exchange reaction under the suppressive conditions with RPA. Interestingly, the EVL protein clearly enhanced the RAD51-mediated strand exchange, in a concentration-dependent manner (Fig. 6, *B* and *C*). No products were observed when the reactions were conducted without the RAD51 protein (Fig. 6*B*, *lane 7*), suggesting that the EVL protein itself did not possess the strand exchange activity. A time course experiment also revealed significant enhancement of the RAD51-mediated strand exchange by the EVL protein (Fig. 6*D*). Therefore, the EVL protein may be a novel stimulation factor for RAD51-mediated strand exchange as well as homologous pairing.

We next tested the effects of the reaction orders on strand exchange. As shown in Fig. 6*E* (*lanes 2* and *3*), the EVL-mediated stimulation of strand exchange was clearly observed when all three proteins, RAD51, RPA, and EVL, were mixed before the addition of ssDNA. Similarly, substantial enhancement was observed when the RAD51 protein was incubated with ssDNA followed by the addition of the RPA and EVL proteins (Fig. 6*E*, *lanes 4* and *5*). A small but clear increase in the products was detected when the RAD51 protein, RPA, and ssDNA were mixed before the addition of the EVL protein (Fig. 6*E*, *lanes 6* and *7*). Preincubation of the RAD51 and EVL proteins with ssDNA before the addition of RPA also enhanced the strand exchange (Fig. 6*E*, *lanes 8* and *9*). Therefore, the EVL protein actually stimulates the RAD51-mediated strand exchange in various reaction orders, although the stimulation efficiencies significantly depend on the reaction order.

It should be noted that the partial ssDNA annealing products (indicated by *asterisks* in Fig. 6) generated by the RAD51 protein were detected under the reaction conditions used in the present study (30 °C). This RAD51-dependent ssDNA annealing product was resolved by heating and was not significantly formed when the reactions were performed at 37 °C (supplemental Fig. 2).

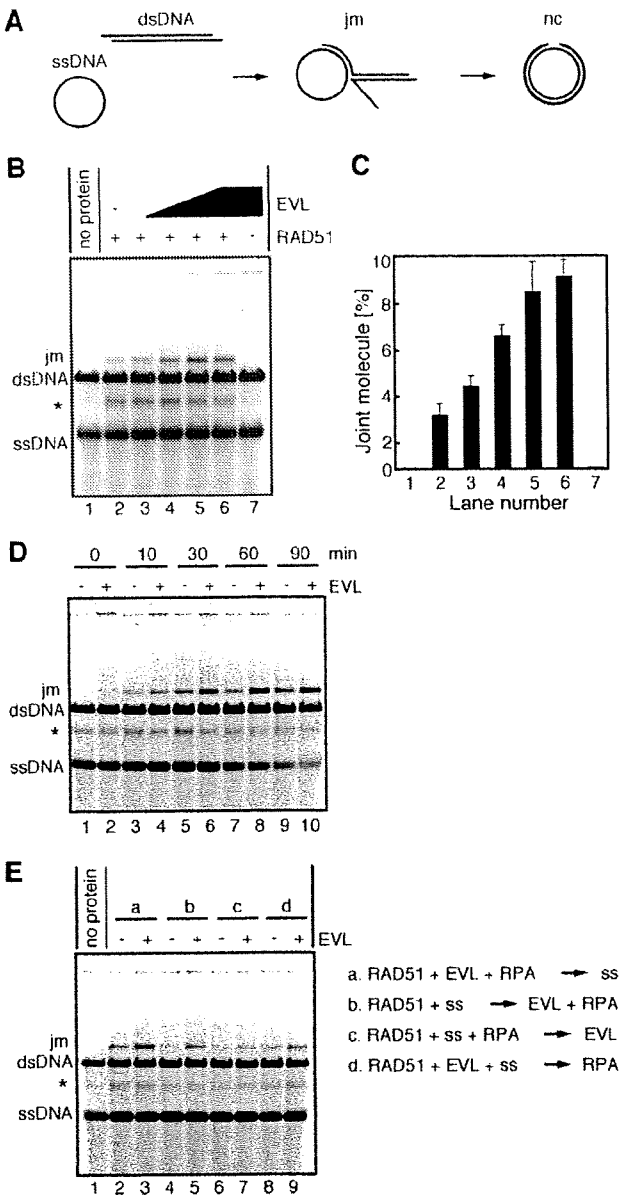

FIGURE 6. **The EVL protein stimulates the RAD51-mediated strand exchange.** *A*, a schematic representation of the strand exchange reaction. The two reaction products, joint molecule and nicked circular DNAs, are denoted as *jm* and *nc*, respectively. *B*, the RAD51 protein (1 μM) and RPA (1 μM) were incubated with the indicated amounts of the EVL protein at 30 °C for 10 min. After this incubation, φX174 circular ssDNA (20 μM) was added to the reaction mixture, which was incubated at 30 °C for 10 min. The reactions were then initiated by the addition of φX174 linear dsDNA (20 μM) and were continued at 30 °C for 60 min. The deproteinized products were separated by 1% agarose gel electrophoresis and were visualized by SYBR Gold (Invitrogen) staining. The *asterisk* indicates the self-annealing products of the ssDNA. The EVL concentrations were 0 μM (*lanes 1 and 2*), 0.25 μM (*lane 3*), 0.5 μM (*lane 4*), 1 μM (*lane 5*), and 2 μM (*lanes 6 and 7*). *Lane 7*, a control experiment without the RAD51 protein. *C*, graphic representation of the experiments shown in *B*. The band intensities of the joint molecule DNA products were quantified, and the average values of three independent experiments are shown with the S.D. values. *D*, time course experiment. The RAD51 protein (1 μM) and RPA (1 μM) were incubated with the EVL protein (1 μM) at 30 °C for 10 min. After this incubation, φX174 circular ssDNA (20 μM) was added to the reaction mixture, which was further incubated at 30 °C for 10 min. The reactions were then initiated by the addition of φX174 linear dsDNA (20 μM) and were continued for the indicated times. The deproteinized products were separated by 1% agarose gel electrophoresis and were visualized by SYBR Gold staining. *E*, the strand exchange assay with various reaction orders. The RAD51 protein (1 μM), RPA (1 μM), the EVL protein (1 μM), and ssDNA were incubated in the indicated reaction orders at 30 °C for 10 min. The reactions were then initiated by the addition of φX174 linear dsDNA (20 μM) and were continued at 30 °C for 60 min. The deproteinized products were separated by 1% agarose gel electrophoresis and were visualized by SYBR Gold staining. The *asterisk* indicates the self-annealing products of the ssDNA.

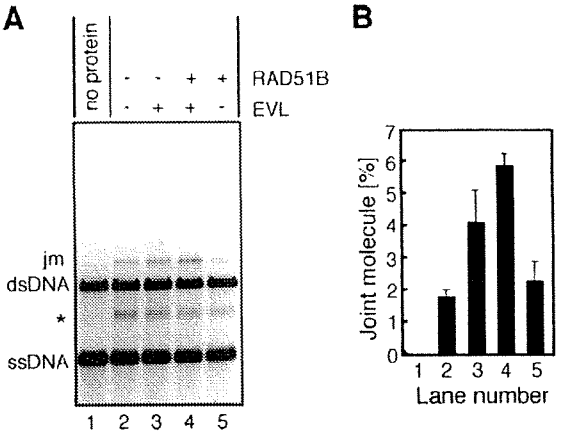

FIGURE 7. **The EVL protein further stimulates the RAD51-mediated strand exchange in the presence of the RAD51B protein.** *A*, the RAD51 protein (1 μM) and RPA (1 μM) were incubated with the EVL protein (0.5 μM) and/or the RAD51B protein (0.5 μM) at 30 °C for 10 min. After this incubation, φX174 circular ssDNA (20 μM) was added to the reaction mixture, which was further incubated at 30 °C for 10 min. The reactions were then initiated by the addition of φX174 linear dsDNA (20 μM) and were continued for 60 min. The deproteinized products were separated by 1% agarose gel electrophoresis and were visualized by SYBR Gold staining. The *asterisk* indicates the self-annealing products of the ssDNA. The EVL concentrations were 0 μM (*lanes 1, 2,* and *5*) and 0.5 μM (*lanes 3* and *4*). The RAD51B protein concentrations were 0 μM (*lanes 1–3*) and 0.5 μM (*lanes 4* and *5*). *B*, graphic representation of the experiments shown in *A*. The band intensities of the joint molecule DNA products (*jm*) were quantified, and the average values of three independent experiments are shown with the S.D. values.

The RAD51B Protein Enhances RAD51-mediated Strand Exchange with the EVL Protein—We next tested whether the RAD51B protein affects RAD51-mediated strand exchange in the presence of the EVL protein, because the RAD51B protein interacts with the EVL protein (Fig. 3, *B* and *D*). The RAD51B protein was added to the reaction mixture in the presence or absence of the EVL protein. We found that the RAD51B protein stimulated RAD51-mediated strand exchange in the presence of the EVL protein (Fig. 7, *A* (*lane 4*) and *B*). In contrast, the RAD51B-dependent stimulation was not observed in the absence of the EVL protein (Fig. 7, *A* (*lane 5*) and *B*). Therefore, the RAD51B protein enhances the RAD51-mediated recombination reaction only in the presence of the EVL protein.

The EVL Protein Promotes Annealing between ssDNA Molecules—We found that the EVL protein possesses robust ssDNA annealing activity. In this assay, complementary ssDNA 49-mers were used as the substrates. As shown in Fig. 8, *A–D*, the EVL protein alone promoted annealing between complementary strands. In contrast, the RAD51B protein alone did not exhibit annealing activity (Fig. 8, *E* (*lanes 2–4*) and *F*). Interestingly, the EVL-mediated annealing was significantly enhanced by the RAD51B protein (Fig. 8, *E* (*lanes 5–8*) and *F*). These results indicated that the EVL protein may be a novel factor that

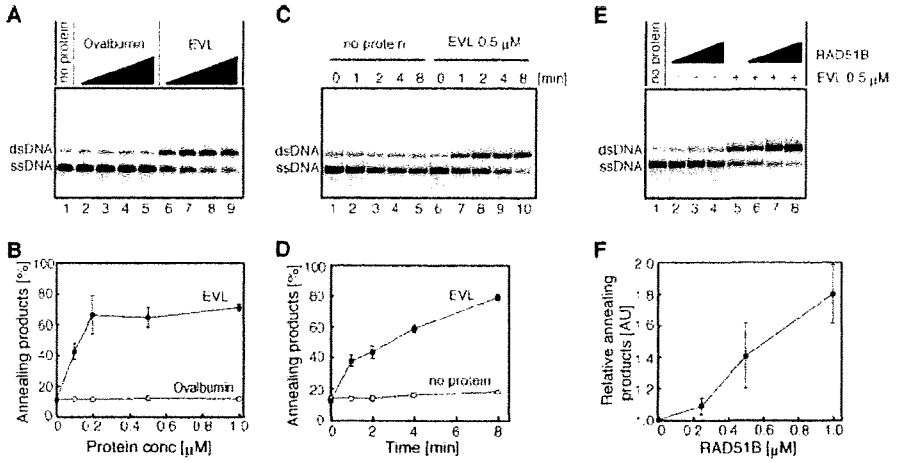

FIGURE 8. **ssDNA annealing activity of the EVL protein.** *A*, protein titration. The EVL protein was first complexed with 2 μM ssDNA, followed by the addition of a complementary ssDNA. The reactions were conducted at 30 °C for 8 min. *Lane 1*, a control experiment without protein; *lanes 6–9*, experiments with the EVL protein. The EVL concentrations were 0 μM (*lane 1*), 0.1 μM (*lane 6*), 0.2 μM (*lane 7*), 0.5 μM (*lane 8*), and 1 μM (*lane 9*). *Lanes 2–5*, negative control experiments with ovalbumin; the amounts of protein were the same as those of the EVL protein, in terms of weight. *B*, graphical representation of the experiments shown in *A*. The band intensities of the annealing products were quantified, and the average values of three independent experiments are shown with the S.D. values. *Closed circles* and *open circles*, experiments with the EVL protein and with ovalbumin, respectively. *C*, time course. *Lanes 1–5*, negative control experiments without the EVL protein. *Lanes 6–10*, experiments with the EVL protein (0.5 μM). Reaction times were 0 min (*lanes 1* and *6*), 1 min (*lanes 2* and *7*), 2 min (*lanes 3* and *8*), 4 min (*lanes 4* and *9*), and 8 min (*lanes 5* and *10*). *D*, graphical representation of the experiments shown in *C*. The band intensities of the annealing products were quantified, and the average values of three independent experiments are shown with the S.D. values. *Closed circles* and *open circles*, experiments with and without the EVL protein, respectively. *E*, effect of the RAD51B protein. The EVL protein was preincubated with or without the RAD51B protein, followed by an incubation with 2 μM ssDNA. The reactions were initiated by the addition of a complementary ssDNA and were conducted at 30 °C for 8 min. *Lanes 1–4*, experiments without the EVL protein; *lanes 5–8*, experiments with the EVL protein. The RAD51B concentrations were 0 μM (*lanes 1* and *5*), 0.25 μM (*lanes 2* and *6*), 0.5 μM (*lanes 3* and *7*), and 1 μM (*lanes 4* and *8*). *F*, graphical representation of the experiments shown in *E*. The band intensities of the annealing products, relative to the experiment in the absence of the RAD51B protein, were quantified, and the average values of three independent experiments are shown with the S.D. values.

functions in the HRR pathway and that the RAD51B protein stimulates the EVL-mediated recombination reactions.

DISCUSSION

The human EVL protein is a member of the Ena/Vasp family, which reportedly functions in cytoplasmic actin dynamics (48). In the present study, we discovered an unexpected function of the EVL protein in the HRR pathway. Specifically, we found that the EVL protein (i) directly binds to the RAD51 and RAD51B proteins, (ii) functions in DSB repair, probably in the RAD51 assembly step on DSB sites, (iii) stimulates RAD51-mediated homologous pairing and strand exchange, and (iv) preferentially binds to ssDNA and promotes ssDNA annealing. We also found that (v) the RAD51B protein enhances the EVL-dependent strand exchange stimulation and ssDNA annealing reactions. These EVL activities discovered in the present study strongly suggest that the EVL protein is a novel activator for the RAD51-mediated homologous recombination reaction.

The biochemical properties of the EVL protein presented here are surprisingly similar to those of the RAD52 protein, which is a prominent RAD51 activator in eukaryotes. The RAD52 protein directly binds to the RAD51 protein (13–15) and stimulates RAD51-mediated homologous pairing (18) and strand exchange (53–55). The RAD52 protein itself possesses robust ssDNA annealing activity (56–59). These functional similarities between the EVL and RAD52 proteins imply that they may have overlapping functions in cells.

In the present study, we found that MMC sensitivity in the EVL knockdown cells was not as remarkable as the MMC sensitivity of the RAD51B knockdown cells. This fact implies that a factor(s) that complements the EVL function may exist. The RAD52 protein, which shares significant biochemical similarity with the EVL protein, may be a factor. In addition, two more paralogs of the EVL protein, MENA and VASP, exist in humans (48) and may also contribute to the functional redundancy of the EVL protein.

The RAD52 knock-out chicken DT40 cells reportedly did not exhibit defects in DSB repair (60). The cells with the double knock-out of the RAD52 and XRCC2 proteins were significantly defective in the HRR pathway (61), indicating that the RAD52 protein has an overlapping function with the XRCC2 protein. The XRCC2 protein forms the BCDX2 complex, which is composed of the RAD51B, RAD51C, RAD51D, and XRCC2 proteins (62, 63), and like the EVL and RAD52 proteins, the BCDX2 complex possesses robust ssDNA annealing activity (64). Therefore, redundant annealing activities may be required in the HRR pathway in higher eukaryotes. The RAD52-mediated annealing is suggested to be important in the second end capture step, just after homologous pairing and strand exchange (65). Therefore, the EVL protein may also function in the second end capture step, in addition to the RAD51 assembly and homologous pairing/strand exchange steps. It is intriguing to study the functional interactions between these ssDNA annealing proteins, such as RAD52, BCDX2, and EVL-RAD51B.

We found that the EVL protein was highly expressed in MCF7 cells. However, we noticed that EVL expression was very low in other cells, such as RPE, HT1080, T47D, HepG2, and HCT116 (data not shown). The rat EVL homologue is reportedly expressed in brain, lung, spleen, thymus, and testis but not in liver, muscle, and prostate (66). Given that the EVL protein is a novel recombination activator for the RAD51-dependent HRR pathway, it may not constitutively function like the RAD51 and RAD51B proteins. The EVL protein may be required for repairing specific DNA lesions in certain tissues or cells, and it may cause tumor malignancy due to inappropriate recombination activation by its overexpression in certain types of tumor cells. The MCF7 cell line,

which robustly expresses the EVL protein, was derived from a breast cancer tumor. Intriguingly, the abnormal expression of the EVL mRNA was also found in another breast cancer tumor (49). Given that EVL overexpression is a source for the malignancy of tumor cells, such as breast cancer, the EVL protein may be a potential target of anti-cancer treatments.

Acknowledgments—We thank Dr. W. Kagawa (RIKEN) for critical reading of the manuscript and also thank the Cs-137 γ-ray Irradiation Facilities for Biological Research, Department of Nuclear Engineering and Management, Graduate School of Engineering, University of Tokyo.

REFERENCES

1. Weinstock, D. M., Richardson, C. A., Elliott, B., and Jasin, M. (2006) *DNA Repair* **5,** 1065–1074
2. Agarwal, S., Tafel, A. A., and Kanaar, R. (2006) *DNA Repair* **5,** 1075–1081
3. Wyman, C., and Kanaar, R. (2006) *Annu. Rev. Genet.* **40,** 363–383
4. Sung, P., and Klein, H. (2006) *Nat. Rev. Mol. Cell Biol.* **7,** 739–750
5. West, S. C. (2003) *Nat. Rev. Mol. Cell Biol.* **4,** 435–445
6. Sung, P. (1994) *Science* **265,** 1241–1243
7. Baumann, P., Benson, F. E., and West, S. C. (1996) *Cell* **87,** 757–766
8. Maeshima, K., Morimatsu, K., and Horii, T. (1996) *Genes Cells* **1,** 1057–1068
9. Gupta, R. C., Bazemore, L. R., Golub, E. I., and Radding, C. M. (1997) *Proc. Natl. Acad. Sci. U. S. A.* **94,** 463–468
10. Symington, L. S. (2002) *Microbiol. Mol. Biol. Rev.* **66,** 630–670
11. Sung, P., Krejci, L., Van Komen, S., and Sehorn, M. G. (2003) *J. Biol. Chem.* **278,** 42729–42732
12. San Filippo, J., Sung, P., and Klein, H. (2008) *Annu. Rev. Biochem.* **77,** 229–257
13. Shen, Z., Cloud, K. G., Chen, D. J., and Park, M. S. (1996) *J. Biol. Chem.* **271,** 148–152
14. Kurumizaka, H., Aihara, H., Kagawa, W., Shibata, T., and Yokoyama, S. (1999) *J. Mol. Biol.* **291,** 537–548
15. Kagawa, W., Kurumizaka, H., Ikawa, S., Yokoyama, S., and Shibata, T. (2001) *J. Biol. Chem.* **276,** 35201–35208
16. Golub, E. I., Kovalenko, O. V., Gupta, R. C., Ward, D. C., and Radding, C. M. (1997) *Nucleic Acids Res.* **25,** 4106–4110
17. Tanaka, K., Hiramoto, T., Fukuda, T., and Miyagawa, K. (2000) *J. Biol. Chem.* **275,** 26316–26321
18. Benson, F. E., Baumann, P., and West, S. C. (1998) *Nature* **391,** 401–404
19. Sigurdsson, S., Van Komen, S., Petukhova, G., and Sung, P. (2002) *J. Biol. Chem.* **277,** 42790–42794
20. Mazina, O. M., and Mazin, A. V. (2004) *J. Biol. Chem.* **279,** 52042–52051
21. Wesoly, J., Agarwal, S., Sigurdsson, S., Bussen, W., Van Komen, S., Qin, J., van Steeg, H., van Benthem, J., Wassenaar, E., Baarends, W. M., Ghazvini, M., Tafel, A. A., Heath, H., Galjart, N., Essers, J., Grootegoed, J. A., Arnheim, N., Bezzubova, O., Buerstedde, J. M., Sung, P., and Kanaar, R. (2006) *Mol. Cell. Biol.* **26,** 976–989
22. Kovalenko, O. V., Golub, E. I., Bray-Ward, P., Ward, D. C., and Radding, C. M. (1997) *Nucleic Acids Res.* **25,** 4946–4953
23. Modesti, M., Budzowska, M., Baldeyron, C., Demmers, J. A., Ghirlando, R., and Kanaar, R. (2007) *Mol. Cell* **28,** 468–481
24. Wiese, C., Dray, E., Groesser, T., San Filippo, J., Shi, I., Collins, D. W., Tsai, M. S., Williams, G. J., Rydberg, B., Sung, P., and Schild, D. (2007) *Mol. Cell* **28,** 482–490
25. Davies, A. A., Masson, J. Y., McIlwraith, M. J., Stasiak, A. Z., Stasiak, A., Venkitaraman, A. R., and West, S. C. (2001) *Mol. Cell* **7,** 273–282
26. Pellegrini, L., Yu, D. S., Lo, T., Anand, S., Lee, M., Blundell, T. L., and Venkitaraman, A. R. (2002) *Nature* **420,** 287–293
27. Yang, H., Jeffrey, P. D., Miller, J., Kinnucan, E., Sun, Y., Thoma, N. H., Zheng, N., Chen, P. L., Lee, W. H., and Pavletich, N. P. (2002) *Science* **297,** 1837–1848
28. Esashi, F., Christ, N., Gannon, J., Liu, Y., Hunt, T., Jasin, M., and West, S. C. (2005) *Nature* **434,** 598–604
29. Galkin, V. E., Esashi, F., Yu, X., Yang, S., West, S. C., and Egelman, E. H. (2005) *Proc. Natl. Acad. Sci. U. S. A.* **102,** 8537–8542
30. Shivji, M. K., Davies, O. R., Savill, J. M., Bates, D. L., Pellegrini, L., and Venkitaraman, A. R. (2996) *Nucleic Acids Res.* **34,** 4000–4011
31. Davies, O. R., and Pellegrini, L. (2007) *Nat. Struct. Mol. Biol.* **14,** 475–483
32. Esashi, F., Galkin, V. E., Yu, X., Egelman, E. H., and West, S. C. (2007) *Nat. Struct. Mol. Biol.* **14,** 468–474
33. Petalcorin, M. I., Galkin, V. E., Yu, X., Egelman, E. H., and Boulton, S. J. (2007) *Proc. Natl. Acad. Sci. U. S. A.* **104,** 8299–8304
34. Mazloum, N., Zhou, Q., and Holloman, W. K. (2007) *Biochemistry* **46,** 7163–7173
35. Mazloum, N., Zhou, Q., and Holloman, W. K. (2007) *Proc. Natl. Acad. Sci. U. S. A.* **105,** 524–529
36. Albala, J. S., Thelen, M. P., Prange, C., Fan, W., Christensen, M., Thompson, L. H., and Lennon, G. G. (1997) *Genomics* **46,** 476–479
37. Rice, M. C., Smith, S. T., Bullrich, F., Havre, P., and Kmiec, E. B. (1997) *Proc. Natl. Acad. Sci. U. S. A.* **94,** 7417–7422
38. Cartwright, R., Dunn, A. M., Simpson, P. J., Tambini, C. E., and Thacker, J. (1998) *Nucleic Acids Res.* **26,** 1653–1659
39. Takata, M., Sasaki, M. S., Sonoda, E., Fukushima, T., Morrison, C., Albala, J. S., Swagemakers, S. M. A., Kanaar, R., Thompson, L. H., and Takeda, S. (2000) *Mol. Cell. Biol.* **20,** 6476–6482
40. Bleuyard, J. Y., Gallego, M. E., Savigny, F., and White, C. I. (2005) *Plant J.* **41,** 533–545
41. Hatanaka, A., Yamazoe, M., Sale, J. E., Takata, M., Yamamoto, K., Kitao, H., Sonoda, E., Kikuchi, K., Yonetani, Y., and Takeda, S. (2005) *Mol. Cell. Biol.* **25,** 1124–1134
42. Osakabe, K., Abe, K., Yamanouchi, H., Takyuu, T., Yoshioka, T., Ito, Y., Kato, T., Tabata, S., Kurei, S., Yoshioka, Y., Machida, Y., Seki, M., Kobayashi, M., Shinozaki, K., Ichikawa, H., and Toki, S. (2005) *Plant Mol. Biol.* **57,** 819–833
43. Yonetani, Y., Hochegger, H., Sonoda, E., Shinya, S., Yoshikawa, H., Takeda, S., and Yamazoe, M. (2005) *Nucleic Acids Res.* **33,** 4544–4552
44. Date, O., Katsura, M., Ishida, M., Yoshihara, T., Kinomura, A., Sueda, T., and Miyagawa, K. (2006) *Cancer Res.* **66,** 6018–6024
45. Sigurdsson, S., Van, Komen, S., Bussen, W., Schild, D., Albala, J. S., and Sung, P. (2001) *Genes Dev.* **15,** 3308–3318
46. Lio, Y. C., Mazin, A. V., Kowalczykowski, S. C., and Chen, D. J. (2003) *J. Biol. Chem.* **278,** 2469–2478
47. Yokoyama, H., Kurumizaka, H., Ikawa, S., Yokoyama, S., and Shibata, S. (2003) *J. Biol. Chem.* **278,** 2767–2772
48. Kwiatkowski, A. V., Gertler, F. B., and Loureiro, J. J. (2003) *Trends Cell Biol.* **13,** 386–392
49. Hu, L. D., Zou, H. F., Zhan, S. X., and Cao, K. M. (2008) *Oncol. Rep.* **19,** 1015–1020
50. Ishida, T., Takizawa, Y., Sakane, I., and Kurumizaka, H. (2008) *Genes Cells* **13,** 91–103
51. Kinebuchi, T., Kagawa, W., Enomoto, R., Tanaka, K., Miyagawa, K., Shibata, T., Kurumizaka, H., and Yokoyama, S. (2004) *Mol. Cell* **14,** 363–374
52. Henricksen, L. A., Umbricht, C. B., and Wold, M. S. (1994) *J. Biol. Chem.* **269,** 11121–11132
53. Sung, P. (1997) *J. Biol. Chem.* **272,** 28194–28197
54. New, J. H., Sugiyama, T., Zaitseva, E., and Kowalczykowski, S. C. (1998) *Nature* **391,** 407–410
55. Shinohara, A., and Ogawa, T. (1998) *Nature* **391,** 404–407
56. Mortensen, U. H., Bendixen, C., Sunjevaric, I., and Rothstein, R. (1996) *Proc. Natl. Acad. Sci. U. S. A.* **93,** 10729–10734
57. Reddy, G., Golub, E. I., and Radding, C. M. (1997) *Mutat. Res.* **377,** 53–59
58. Sugiyama, T., New, J. H., and Kowalczykowski, S. C. (1998) *Proc. Natl. Acad. Sci. U. S. A.* **95,** 6049–6054
59. Kagawa, W., Kagawa, A., Saito, K., Ikawa, S., Shibata, T., Kurumizaka, H., and Yokoyama, S. (2008) *J. Biol. Chem.* **283,** 24264–24273
60. Yamaguchi-Iwai, Y., Sonoda, E., Buerstedde, J. M., Bezzubova, O., Morrison, C., Takata, M., Shinohara, A., and Takeda, S. (1998) *Mol. Cell. Biol.* **18,** 6430–6435
61. Fujimori, A., Tachiiri, S., Sonoda, E., Thompson, L. H., Dhar, P. K.,

Hiraoka, M., Takeda, S., Zhang, Y., Reth, M., and Takata, M. (2001) *EMBO J.* **20,** 5513–5520
62. Masson, J. Y., Tarsounas, M. C., Stasiak, A. Z., Stasiak, A., Shah, R., McIlwraith, M. J., Benson, F. E., and West, S. C. (2001) *Genes Dev.* **15,** 3296–3307
63. Schild, D., Lio, Y. C., Collins, D. W., Tsomondo, T., and Chen, D. (2000) *J. Biol. Chem.* **275,** 16443–16449
64. Yokoyama, H., Sarai, N., Kagawa, W., Enomoto, R., Shibata, T., Kurumizaka, H., and Yokoyama, S. (2004) *Nucleic Acids Res.* **32,** 2556–2565
65. McIlwraith, M. J., and West, S. C. (2008) *Mol. Cell* **29,** 510–516
66. Ohta, S., Mineta, T., Kimoto, M., and Tabuchi, K. (1997) *Biochem. Biophys. Res. Commun.* **237,** 307–312

ARTICLE IN PRESS

Cancer Letters xxx (2010) xxx–xxx

Contents lists available at ScienceDirect

Cancer Letters

journal homepage: www.elsevier.com/locate/canlet

Edaravone, a known free radical scavenger, enhances X-ray-induced apoptosis at low concentrations

N. Sasano [a,b], A. Enomoto [b], Y. Hosoi [c], Y. Katsumura [d], Y. Matsumoto [e], A. Morita [f], K. Shiraishi [a], K. Miyagawa [b], H. Igaki [a], K. Nakagawa [a,*]

[a] Department of Radiology, Graduate School of Medicine, The University of Tokyo, 7-3-1, Hongo, Bunkyo-ku, Tokyo 113-8655, Japan
[b] Laboratory of Molecular Radiology, Center for Disease Biology and Integrative Medicine, Faculty of Medicine, The University of Tokyo, 7-3-1, Hongo, Bunkyo-ku, Tokyo 113-0033, Japan
[c] School of Health Sciences, Faculty of Medicine, Niigata University, 1, Asahimachi-dori, Niigata, Niigata 951-8510, Japan
[d] Nuclear Engineering Research Laboratory, Graduate School of Engineering, The University of Tokyo, The University of Tokyo, 7-3-1, Hongo, Bunkyo-ku, Tokyo 113-0033, Japan
[e] Mass Transmutation Engineering Division, Research Laboratory for Nuclear Reactors, Tokyo Institute of Technology, 2-12-1, Oh-Okayama, Meguro-ku, Tokyo 152-0033, Japan
[f] Department of Applied Biological Science, Faculty of Science and Technology, Tokyo University of Science, 1-3, Kagurazaka, Shinjuku-ku, Tokyo 162-8601, Japan

ARTICLE INFO

Article history:
Received 13 October 2009
Received in revised form 19 December 2009
Accepted 23 December 2009
Available online xxxx

Keywords:
Edaravone
Radiosensitizer
Apoptosis
p53

ABSTRACT

Edaravone has been reported to have a radioprotective effect at high concentrations. We now report that a lower dose of edaravone enhanced X-ray-induced apoptosis of some cell lines harboring p53 wild-type status, such as MOLT-4, Nalm-6, and HepG2. The knock-down of p53 using siRNA in MOLT-4 cells abolished the radiosensitizing effect of edaravone. Enhanced phosphorylations of p53 at Ser 15 and Ser 20 and up-regulation of PUMA, a p53 target protein, were observed after X-irradiation in the presence of edaravone. We conclude that the low dose of edaravone sensitized cells to X-irradiation by promoting the p53-dependent apoptotic signaling pathway.

1. Introduction

Edaravone (MCI-186; 3-methyl-1-phenyl-2-pyrazolin-5-one) is a drug widely used clinically for the treatment of acute cerebral infarction [1] and is known to scavenge free radicals as an electron donor [2]. We previously reported that in the human T-cell leukemia cell line, MOLT-4, 3 mg/ml of edaravone suppressed X-ray-induced apoptosis by inhibiting both reactive oxygen species (ROS) and p53 [3]. The MOLT-4 cell line is highly sensitive to X-rays and undergoes p53- and caspase-dependent apoptosis, showing nuclear condensation and DNA fragmentation [4]. p53 is a well-studied transcription factor associated with the determination of the cells to undergo apoptosis or other fates after DNA damage. After DNA damage, p53 stability is increased by phosphorylation, and the accumulated p53 induces the transcription of its target genes [5], including the p53-upregulated modulator of apoptosis (PUMA). PUMA is a BH3-only protein belonging to the Bcl-2 family that regulates apoptosis and plays a key functional role in the process of p53-mediated apoptosis [6–9]. Overexpressing a dominant-negative form of p53 in MOLT-4 cells results in resistance to radiation-induced apoptosis [10].

Various compounds have been reported to be effective as radiosensitizers, such as wortmannin. Wortmannin is an extensively studied inhibitor of the phosphatidylinositol 3-kinase family, ataxia telangiectasia mutated (ATM) and DNA-dependent protein kinase (DNA-PK). Wortmannin has also been reported to enhance X-ray-induced apoptosis through the inhibition of DNA repair [11,12]. Tomita et al. [13] also demonstrated that wortmannin enhances

* Corresponding author.
E-mail address: nakagawa-rad@umin.ac.jp (K. Nakagawa).

0304-3835/$ - see front matter © 2009 Elsevier Ireland Ltd. All rights reserved.
doi:10.1016/j.canlet.2009.12.020

Please cite this article in press as: N. Sasano et al., Edaravone, a known free radical scavenger, enhances X-ray-induced apoptosis at low concentrations, Cancer Lett. (2010), doi:10.1016/j.canlet.2009.12.020

X-ray-induced apoptosis possibly through the JNK/SAPK pathway in MOLT-4 cells.

Because the clinical concentration of edaravone in human blood is estimated to be approximately 1000-fold lower than that used in the previous study [14], we sought to determine the effect of lower concentrations of edaravone on X-ray-induced apoptosis. The presumption was that lower concentrations of edaravone would show a milder radioprotective effect. However, contrary to our expectations, we found that even a lower dose of edaravone enhanced the X-ray-induced apoptosis through the p53 pathway.

2. Materials and methods

2.1. Cell culture

Human T-cell leukemia MOLT-4 cells, MOLT-4 stable transfectants overexpressing short hairpin (sh)-type p53 small interfering RNA (siRNA) (p53 knock-down MOLT-4), human pre-B-cell leukemia Nalm-6 cells, and human hepatocellular carcinoma (HepG2) cells were cultured in Dulbecco's Modified Eagle Medium (Sigma) containing 5% fetal bovine serum (Hyclone) and antibiotics (100 units/ml of penicillin/streptomycin), and incubated at 37 °C in a humidified atmosphere of 5% CO_2 and 95% air. To generate p53 knock-down MOLT-4 cells, MOLT-4 cells were transfected by electroporation (Gene Pulsar II, Bio-Rad; 0.25 kV, 950 microfarads) with the ApaLI-linearized vectors (GeneSuppressor System, p53 siRNA plasmid and the negative control shRNA plasmid, IMGENEX), and selected on 0.16% soft agar culture containing 0.8 mg/ml G418 for 3 weeks.

2.2. Chemicals

Edaravone was kindly provided by the Mitsubishi Tanabe Pharma Corporation (Tokyo, Japan). Edaravone (52.5 mg) was dissolved in 192.5 μl of 2 M NaOH and 1.05 ml of DDW, and then adjusted to pH 8.8 with 2 M HCl. Finally, physiological saline was added to adjust the final concentration of edaravone to 30 mg/ml. Edaravone was added to the cells 5 min before X-irradiation.

2.3. X-irradiation

X-irradiation was performed with an X-ray generator (Pantak HF 350, Shimadzu) at 200 kVp and 20 mA, with a filter of 0.5 mm Cu and 1 mm Al, and at a dose rate of 1.35–1.40 Gy/min.

2.4. Dye exclusion tests

One hundred microliters of cell suspension (approximately 5×10^5 cells/ml) was mixed with 25 μl of 1% erythrosin B in PBS. The numbers of stained (dead) cells and unstained (live) cells were counted and the viability (%) was calculated as follows:

Viability(%)
= (number of unstained cells/total cell number) × 100

2.5. Annexin V binding assay

The extent of apoptosis was determined by Annexin V-FITC and propidium iodine (PI) staining, using the MEBCYTO Apoptosis Kit (MBL). Flow cytometric analysis was carried out with an EPICS flow cytometer (XL System II, Beckman Coulter), using a single laser emitting excitation light at 488 nm. In the FITC/PI diparametric plot, cells in quadrant four (upper FITC/ lower PI) were considered to be in the early stage of apoptosis. More than 5000 cells were subjected to the analysis.

2.6. Quantification of intracellular ROS

The amount of intracellular ROS production was measured by chloromethyl-2′, 7′-dichlorodihydro-fluorescein diacetate (CM-H_2-DCFDA, Molecular Probes). MOLT-4 cells were incubated in the dark with approximately 5 μg/ml of probe CM-H_2-DCFDA for an hour, and the fluorescence intensity was analyzed by an EPICS flow cytometer (XL System II, Beckman Coulter) using a laser excitation and emission wavelength of 492–495 nm and 517–527 nm, respectively.

2.7. Western blotting

Cells were lysed in a SDS sample buffer (1% SDS, 3% β-mercaptoethanol, 5% glycerol, 62.5 mM Tris–HCl, pH 6.8). Proteins were separated by 10% or 15% SDS–PAGE and were transferred onto polyvinylidene difluoride membranes (Immobilon, Millipore). After blocking for 30 min in 5% skim milk in TBS (20 mM Tris–HCl, pH 7.5, 150 mM NaCl) supplemented with 0.05% Tween-20 (TBS-T), the membranes were incubated overnight at 4 °C in TBS-T containing 5% skim milk and primary antibodies. The primary antibodies were anti-p53 (clone DO-1, Santa Cruz Biotechnology), anti-phospho p53 at Ser 15 (Calbiochem), Ser 6, Ser 9, Ser 20, and Ser 392 (cell signaling), anti-cleaved caspase-3 (cell signaling), anti-caspase-7 (MBL), anti-PUMA (Calbiochem), and anti-β-actin (Sigma, AC-15). After rinsing three times with TBS-T, the membranes were incubated for 2 h at room temperature in TBS-T containing 5% skim milk and secondary antibodies conjugated with horseradish peroxidase (DAKO). The membranes were then washed three times with TBS-T, once with TBS, and developed using an ECL-plus kit (GE Healthcare). The signals were obtained by exposure to X-ray films (Hyperfilm MP, GE Healthcare).

2.8. Statistical analysis

All experiments were repeated at least three times. The results are expressed as the mean ±standard deviation (SD) of the mean. All laboratory data were evaluated according to standard statistical methods, using commercially available computer programs such as Microsoft Excel 2000. Statistical differences were determined using the Student's *t*-test. In all tests, *P* values less than 0.05 were considered statistically significant.

Please cite this article in press as: N. Sasano et al., Edaravone, a known free radical scavenger, enhances X-ray-induced apoptosis at low concentrations, Cancer Lett. (2010), doi:10.1016/j.canlet.2009.12.020

3. Results

3.1. Edaravone significantly enhances X-ray-induced cell death at low concentrations

First, the cytotoxicity of edaravone was determined by using the dye exclusion test [3]. Cell viability was examined in cultures treated with 0.15, 0.75, 1.5, 3, and 6 mg/ml edaravone. With concentrations of edaravone up to 3 mg/ml, the cell viabilities were more than 60%, which was considered acceptable (Fig. 1A). On the other hand, when treated with 6 mg/ml edaravone, cell viability was less than 30% and this was considered overly cytotoxic (Fig. 1A). These results are consistent with the previous report [3].

To determine the effect of edaravone on X-ray-induced cell death, MOLT-4 cells were treated with various concentrations of edaravone, and then subjected to 2 Gy X-irradiation 5 min later. Cell viabilities were determined 20 h after the treatment. When MOLT-4 cells were X-irradiated without edaravone, the cell viability was 36.2 ± 6.3% (Fig. 1A). When MOLT-4 cells were X-irradiated in the presence of edaravone at concentrations of 0.15, 0.75, and 1.5 mg/ml, the cell viabilities were 9.7 ± 2.1%, 5.7 ± 3.5%, and 7.2 ± 6.3%, respectively (Fig. 1A). These results were significantly lower than that in the absence of edaravone ($P < 0.05$). The enhancement of X-ray-induced cell death was observed in a time- and dose-dependent manner ($P < 0.05$) (Fig. 1B and C). These results indicate that low doses of edaravone enhanced X-ray-induced cell death. Considering the cytotoxicity of edaravone (Fig. 1A), the combined effect of these concentrations of edaravone and X-irradiation on MOLT-4 cell viability was considered supra-additive. On the other hand, when MOLT-4 cells were X-irradiated in combination with 2.7 or 3 mg/ml of edaravone, the cell viability increased significantly ($P < 0.05$) (Fig. 1A), which was compatible with the previous report [3]. Because 0.75 mg/ml of edaravone appeared to enhance X-ray-induced MOLT-4 cell death most effectively, this dose was used for all subsequent experiments in this study.

Although not as remarkable as noted in MOLT-4 cells, the radiosensitizing effect of edaravone was also observed in human pre-B-cell leukemia Nalm-6 and hepatocellular carcinoma HepG2 cells ($P < 0.05$) (Fig. 2A and B). Thus, the radiosensitizing effect of a low dose of edaravone is not limited to MOLT-4 cells, but is observed in cells with p53 wild-type status.

To determine whether DMSO (dimethylsulfoxide), another free radical scavenger, has a similar radiosensitizing effect in low doses, a dye exclusion test was performed on MOLT-4 cells treated with 0.2% or 1% DMSO, and then subjected to X-irradiation. The viability of the cells treated with 1% DMSO before X-irradiation was significantly greater than that of the cells treated only with X-irradiation ($P < 0.05$), indicating that 1% DMSO had a radioprotective effect. On the other hand, the viability of the cells treated with 0.2% DMSO before X-irradiation was almost the same as that of the cells treated only with X-irradiation (Fig. 2C). These results indicate that low doses of free radical scavengers do not always show the radiosensitizing effect.

3.2. Low dose of edaravone (0.75 mg/ml) enhances X-ray-induced MOLT-4 cell death by promoting apoptosis

To determine whether the radiosensitizing effect of edaravone is mediated by apoptosis, the effect of edaravone on the induction of apoptosis was examined by using flow cytometric studies with Annexin V-PI staining. When MOLT-4 cells were treated with either edaravone or 2 Gy X-ray, the percentages of Annexin V+/PI− cells in the early stage of apoptosis were 2.04 ± 0.21% and 12.43 ± 1.96%, respectively (Fig. 3A and C). When MOLT-4 cells were subjected to 2 Gy X-irradiation in addition to edaravone, the result was 39.57 ± 4.48% (Fig. 3B and C). This indicated that adding 0.75 mg/ml edaravone significantly increased the frequency of X-ray-induced apoptosis ($P < 0.05$), and that the combined effect of edaravone and X-irradiation was supra-additive. The next investigation was on the effect of edaravone on the activation of caspase-3 and -7, which are known as apoptotic effectors and play crucial roles in the execution of apoptosis [15]. Treatment with X-irradiation combined with edaravone resulted in an earlier induction of the active forms of caspase-3 and -7. With X-irradiation alone however, the same results were not obtained until 8 h after the treatment (Fig. 3D). These data indicate that the radiosensitizing effect of a low dose of edaravone is due to the enhancement of apoptosis.

3.3. Effects of edaravone on the production of intracellular ROS

CM-H_2-DCFDA, a fluorescence-based probe recently developed to detect the intracellular production of ROS, was used in a flow cytometry sys-

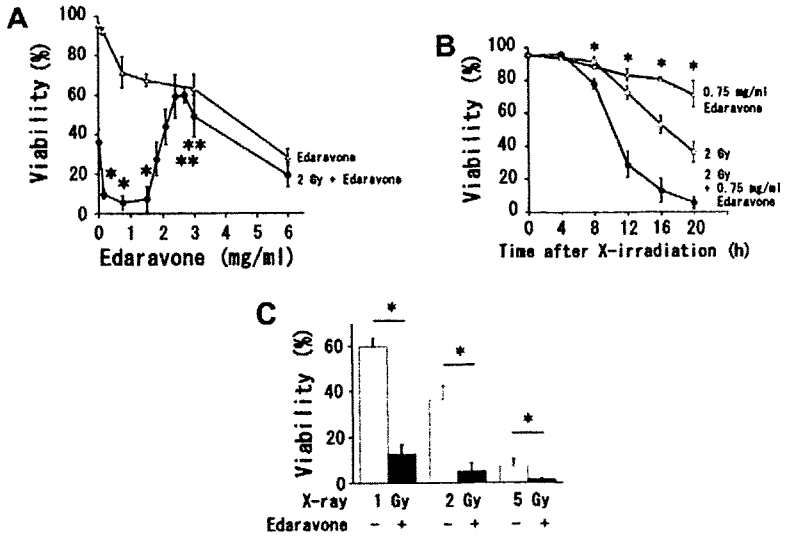

Fig. 1. Low concentrations of edaravone enhanced X-ray-induced cell death in MOLT-4 cells. (A) Cytotocixity of edaravone and effects of various concentrations of edaravone on 2 Gy X-ray-induced cell death are shown. Cell viabilities were determined 20 h after treatment with the indicated concentrations of edaravone with or without X-irradiation. $^{*}P < 0.05$, meaning significantly lower than that of the X-irradiated cells in the absence of edaravone. $^{**}P < 0.05$, meaning significantly higher than that of the X-irradiated cells in the absence of edaravone. (B) The time-course cell viability after treatment with 2 Gy X-irradiation and/or 0.75 mg/ml edaravone. $^{*}P < 0.05$, meaning that the viability of the X-irradiated cells in the absence of edaravone is significantly higher than that of the X-irradiated cells in the presence of 0.75 mg/ml edaravone. (C) X-ray-dose response of cell death in the absence or presence of 0.75 mg/ml edaravone. $^{*}P < 0.05$.

Please cite this article in press as: N. Sasano et al., Edaravone, a known free radical scavenger, enhances X-ray-induced apoptosis at low concentrations, Cancer Lett. (2010), doi:10.1016/j.canlet.2009.12.020

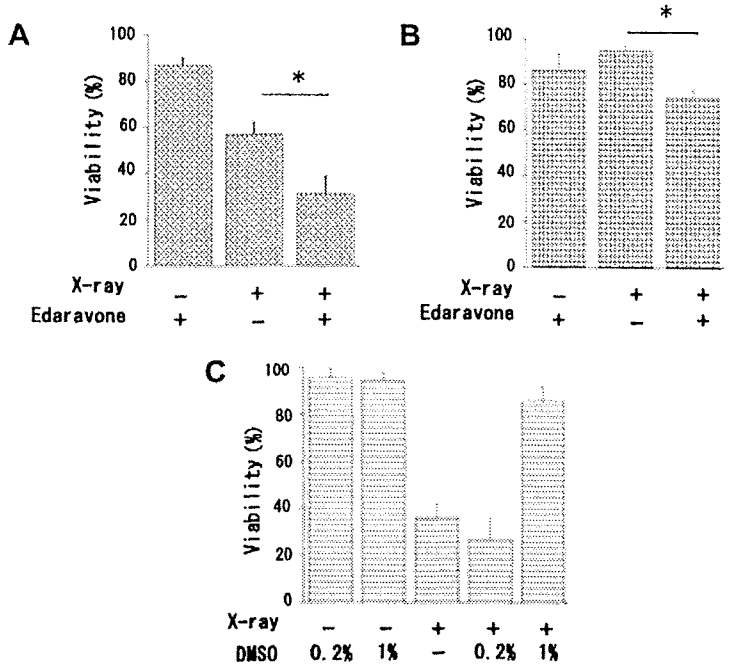

Fig. 2. Low concentrations of edaravone also enhanced X-ray-induced cell death in Nalm-6 (A) and HepG2 (B) cells. In Nalm-6 and HepG2 cells, cell viabilities were determined by dye exclusion test with erythrosine B 20 h after the treatment with 0.75 mg/ml edaravone and/or 2 Gy X-irradiation. $^{*}P < 0.05$. (C) Another free radical scavenger, DMSO, did not show the radiosensitizing effect at a low dose. Cell viability of MOLT-4 was determined 20 h after X-irradiation in the absence or presence of DMSO.

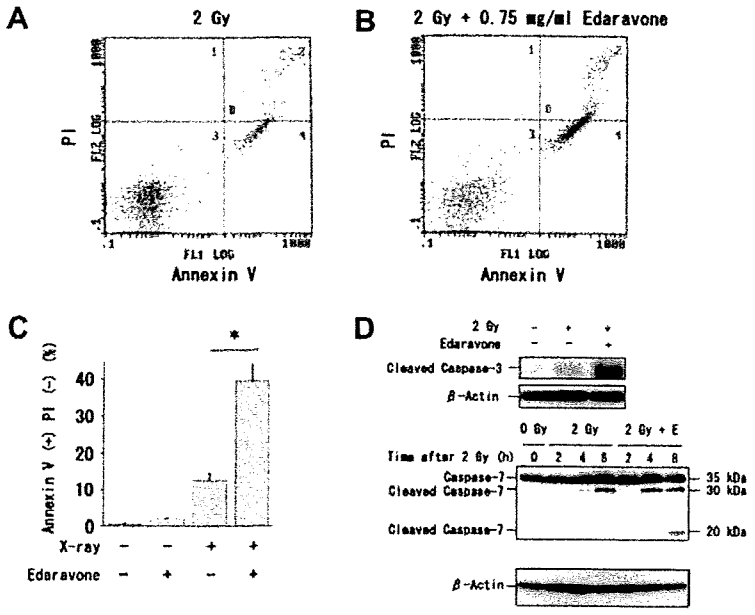

Fig. 3. A low dose of edaravone enhanced X-ray-induced apoptosis. (A–C) Apoptosis was quantified by Annexin V-PI staining. Cells were harvested 8 h after each treatment (2 Gy X-irradiation and/or 0.75 mg/ml edaravone). (A) Two Gy X-irradiation only. (B) Two Gy X-irradiation and 0.75 mg/ml edaravone. (C) The percentage of the Annexin V+/PI− cells is indicated. $^{*}P < 0.05$. (D) Cells were X-irradiated in the absence or presence of 0.75 mg/ml edaravone (E), then harvested at the indicated times. Western blot analysis was performed using anti-cleaved caspase-3 and anti-caspase-7. β-Actin as a loading control is shown.

Please cite this article in press as: N. Sasano et al., Edaravone, a known free radical scavenger, enhances X-ray-induced apoptosis at low concentrations, Cancer Lett. (2010), doi:10.1016/j.canlet.2009.12.020

tem to study the effect of edaravone on the X-ray-induced production of intracellular ROS [16]. CM-H_2-DCFDA is passively diffused into and trapped within the cells, and is deacetylated by intracellular esterases. It is subsequently oxidized to a fluorescent product in the presence of intracellular ROS. The oxidation of CM-H_2-DCFDA can be monitored as a convenient determinant of the level of intracellular oxidative stress. X-irradiation at 20 Gy induced an approximately 11-fold increase in basal CM-H_2-DCFDA fluorescence, which was significantly suppressed by adding 0.75 mg/ml edaravone 5 min before X-irradiation ($P < 0.05$) (Fig. 4A). Moreover, the suppressive effect was even greater when 3 mg/ml edaravone was added ($P < 0.05$). This result indicates that the radiosensitizing effect of edaravone is not mediated by promoting ROS generation.

3.4. p53 is involved in the radiosensitizing effect of a low dose (0.75 mg/ml) of edaravone

To determine whether p53 is involved in the radiosensitizing effect of edaravone, we used one of two stable p53 knock-down transformants, which were generated using a vector that overexpressed p53 siRNA [17]. A clone was used which showed a better suppression of p53. It was reconfirmed that this clone showed significantly lower levels of p53 expression than the wild-type MOLT-4 cells even after X-irradiation with or without edaravone (Fig. 4B). This clone was X-irradiated at 2 Gy with or without edaravone and the cells were subjected to the dye exclusion test. Differences of cell viabilities at 20 h after X-irradiation for the cells untreated or treated with edaravone were not significant, i.e., 88.63 ± 2.02% and 86.13 ± 4.75%, respectively (Fig. 4C). The suppression of p53 by siRNA abolished the radiosensitizing effect of edaravone. Therefore, these results suggest that the p53 pathway is involved in the radiosensitizing effect of edaravone. Next, the effects of edaravone were analyzed on the accumulation or phosphorylation of p53 by Western blot analysis with total or phospho-specific antibodies. The results showed that edaravone enhanced the phosphorylation of p53 at Ser 15 and Ser 20 (Fig. 4D). Since phosphorylation of p53 at Ser 15 and 20 has been reported to play an important role in apoptosis induced by DNA damage [18], our results suggest that edaravone specifically stimulates DNA damage-induced apoptosis signaling. On the other hand, the accumulation of p53 and its phosphorylation at Ser 6, Ser 9, and Ser 392 induced by X-irradiation did not increase significantly in the presence of edaravone (Fig. 4D).

Since edaravone enhances DNA damage-induced apoptosis, we next investigated the expression of p53 target genes, especially an apoptosis-related protein PUMA, which is a pro-apoptotic Bcl-2 family protein and induced by DNA damage [8,19]. The expression of PUMA was apparent 4 h after 2 Gy X-irradiation, and it increased significantly when a low dose of edaravone was added before X-irradiation (Fig. 4E). On the other hand, the expression of PUMA induced by X-irradiation was suppressed in the presence of 3 mg/ml edaravone (Fig. 4E), which is compatible with its radioprotective effect shown previously for that dose [3]. The expression of PUMA in the p53 knock-down transformants was not as apparent as that in wild-type MOLT-4 cells after X-irradiation in the presence or absence of edaravone (Fig. 4B). The results indicate that the low dose of edaravone enhanced the expression of the p53 target gene PUMA, and suggest that the enhanced expression contributed to the promotion of apoptosis.

4. Discussion

We found that a low dose of edaravone enhanced X-ray-induced cell death (Fig. 1A–C). This radiosensitizing effect was observed in multiple p53 wild-type cell lines (Figs.

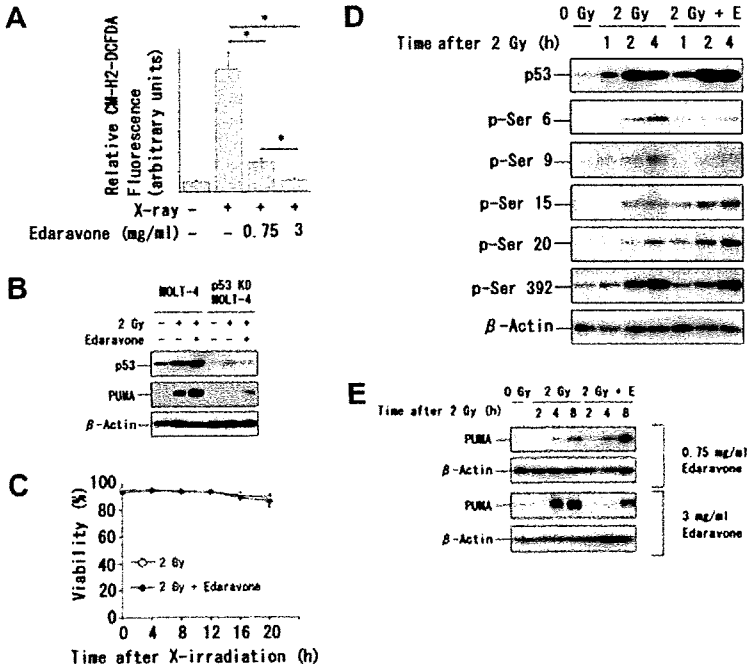

Fig. 4. p53 is involved in the radiosensitizing effect of low dose of edaravone. (A) Intracellular ROS determined by the CM-H_2-DCFDA flow cytometry system. The amount of intracellular ROS after treatment (20 Gy X-irradiation with or without 0.75 or 3 mg/ml edaravone) is shown. Edaravone was added 5 min before X-irradiation. The ROS production of each sample was quantified as described in Materials and methods. Data shown are means ± SD from at least three independent experiments. *$P < 0.05$. (B) MOLT-4 cells and its stable transformants (p53 knock-down (KD) MOLT-4 cells) were X-irradiated with or without 0.75 mg/ml edaravone, then subjected to Western blot analysis with p53 or PUMA antibody. β-Actin is used as a loading control. (C) MOLT-4 and p53 knock-down MOLT-4 cells were X-irradiated with 0.75 mg/ml edaravone, and harvested for the indicated times. (D) Effects of the low dose of edaravone (E) on X-ray-induced accumulation or phosphorylations of p53 at Ser 6, Ser 9, Ser 15, Ser 20, or Ser 392. β-Actin was used as a loading control. (E) Effects of edaravone on X-ray-induced induction of p53 targets, PUMA. MOLT-4 cells were X-irradiated in the absence or presence of the indicated concentrations of edaravone, and harvested at the indicated times. β-Actin was used as a loading control.

Please cite this article in press as: N. Sasano et al., Edaravone, a known free radical scavenger, enhances X-ray-induced apoptosis at low concentrations, Cancer Lett. (2010), doi:10.1016/j.canlet.2009.12.020

1A–C, 2A and B), but not in p53 knock-down MOLT-4 (Fig. 4C). The radiosensitization was mainly caused by enhancing apoptosis (Fig. 3A–D), although ROS was partially suppressed (Fig. 4A), indicating that the radiosensitizing effect was not due to enhancement of ROS generation. We next investigated whether DNA damage signaling pathways were up-regulated, especially the p53-dependent pathway. Although p53 accumulation did not change after X-irradiation in the absence or presence of edaravone, the phosphorylation of p53 at Ser 15 and Ser 20 was enhanced by adding edaravone before X-irradiation (Fig. 4D). Moreover, up-regulation of the p53 target gene, PUMA, was observed with the addition of a low dose of edaravone (Fig. 4E).

PUMA has been reported to play a causal role in p53-dependent apoptosis. Villunger et al. [8] demonstrated that DNA damage-induced apoptosis decreased in PUMA-disrupted mouse fibroblasts and loss of PUMA protected lymphocytes from cell death. The expression of PUMA, which is induced by p53, might contribute to the radiosensitizing effect of edaravone. Our results suggest that the enhancement of phosphorylations of p53 alter the expression pattern of the p53 target genes, causing the promotion of apoptosis.

A question which remains to be answered is why a low dose of edaravone enhances X-ray-induced apoptosis even though it partially eliminates the intracellular ROS generated by X-irradiation (Fig. 4A). In the previous study, a higher dose (3 mg/ml) of edaravone completely eliminated intracellular ROS generated by X-irradiation, causing the suppression of p53 accumulation and phosphorylation at Ser15 [3]. In the present study, p53 phosphorylation at Ser 15 and Ser 20 were enhanced in the presence of edaravone after X-irradiation. The phosphorylation of p53 at Ser 15 or Ser 20 has been shown to be mediated by the ATM, leading to p53 activation [20]. A low dose of edaravone might effect on the activity of ATM or the related protein kinases, resulting in the enhanced phosphorylation of p53, at least at Ser 15 and Ser 20.

We conclude that a low dose of edaravone (0.75 mg/ml) used in this study enhanced X-ray-induced apoptosis by modifying p53 transcriptional activity. The results of the current study may have important clinical implications for radiation therapy.

5. Conflicts of Interest

None declared.

Acknowledgements

We thank all the members of our laboratory for their help and encouragement. We also thank Dr. T. Kondo (University of Toyama) for various suggestions and instructions. This study was supported in part by the Mitsubishi Tanabe Pharma Corporation (Tokyo, Japan). This study was also supported in part by the Radiation Effects Association.

References

[1] Edaravone Acute Infarction Study Group, Effect of a novel free radical scavenger edaravone (MCI-186) on acute brain infarction. Randomized placebo-controlled double-blind study at multicenters, Cerebrovasc. Dis. 15 (2003) 222–229.
[2] S. Abe, K. Kirima, K. Tsuchiya, M. Okamoto, T. Hasegawa, H. Houchi, M. Yoshizumi, T. Tamaki, The reaction rate of edaravone (3-methyl-1-phenyl-2-pyrazolin-5-one (MCI-186)) with hydroxyl radical, Chem. Pharm. Bull. (Tokyo) 52 (2004) 186–191.
[3] N. Sasano, A. Enomoto, Y. Hosoi, Y. Katsumura, Y. Matsumoto, K. Shiraishi, K. Miyagawa, H. Igaki, K. Nakagawa, Free radical scavenger edaravone suppresses X-ray-induced apoptosis through p53 inhibition in MOLT-4 cells, J. Radiat. Res. (Tokyo) 48 (2007) 495–503.
[4] A. Enomoto, N. Suzuki, Y. Kang, K. Hirano, Y. Matsumoto, J. Zhu, A. Morita, Y. Hosoi, K. Sakai, H. Koyama, Decreased c-Myc expression and its involvement in X-ray-induced apoptotic cell death of human T-cell leukemia cell line MOLT-4, Int. J. Radiat. Biol. 79 (2003) 589–600.
[5] G.M. Wahl, A.M. Carr, The evolution of diverse biological responses to DNA damage: insights from yeast and p53, Nature Cell Biol. 3 (2001) E277–E286.
[6] J.R. Jeffers, E. Parganas, Y. Lee, C. Yang, J. Wang, J. Brennan, K.H. MacLean, J. Han, J.N. Ihle, P.J. McKinnon, J.L. Cleveland, G.P. Zambetti, Puma is an essential mediator of p53-dependent and- independent apoptotic pathways, Cancer Cell 4 (2003) 321–328.
[7] K. Nakano, K.H. Vousden, PUMA a novel proapoptotic gene is induced by p53, Mol. Cell 7 (2001) 683–694.
[8] A. Villunger, E.M. Michalak, L. Coultas, F. Müllauer, G. Böck, M.J. Ausserlechner, J.M. Adams, A. Strasser, p53- and drug-induced apoptotic responses mediated by BH3-only proteins puma and noxa, Science 302 (2003) 1036–1038.
[9] J. Yu, Z. Wang, K.W. Kinzler, B. Vogelstein, L. Zhang, PUMA mediates the apoptotic response to p53 in colorectal cancer cells, Proc. Natl. Acad. Sci. USA 100 (2003) 1931–1936.
[10] H. Nakano, M. Kohara, K. Shinohara, Evaluation of the relative contribution of p53-mediated pathway in X-ray-induced apoptosis in human leukemic MOLT-4 cells by transfection with a mutant p53 gene at different expression levels, Cell Tissue Res. 306 (2001) 101–106.
[11] K.E. Rosenzweig, M.B. Youmell, S.T. Palayoor, B.D. Price, Radiosensitization of human tumor cells by the phosphatidylinositol 3-kinase inhibitors wortmannin and LY294002 correlates with inhibition of DNA-dependent protein kinase and prolonged G2-M delay, Clin. Cancer Res. 3 (1997) 1149–1156.
[12] J.N. Sarkaria, R.S. Tibbetts, E.C. Busby, A.P. Kennedy, D.E. Hill, R.T. Abraham, Inhibition of phosphoinositide 3-kinase related kinases by the radiosensitizing agent wortmannin, Cancer Res. 58 (1998) 4375–4382.
[13] M. Tomita, N. Suzuki, Y. Matsumoto, A. Enomoto, H.L. Yin, Y. Hosoi, K. Hirano, K. Sakai, Wortmannin-enhanced X-ray-induced apoptosis of human T-cell leukemia MOLT-4 cells possibly through the JNK/SAPK pathway, Radiat. Res. 160 (2003) 467–477.
[14] H. Shibata, S. Arai, M. Izawa, M. Murasaki, Y. Takamatsu, O. Izawa, C. Takahashi, M. Tanaka, Phase I clinical study of MCI-186 (Edaravone; 3-methyl-1-phenyl-2-pyrazolin-5-one) in healthy volunteers: safety and pharmacokinetics of single and multiple administration, Jpn. J. Clin. Pharmacol. Ther. 29 (1998) 863–876.
[15] S. Kumar, Caspase function in programmed cell death, Cell Death Differ. 14 (2007) 32–43.
[16] T. Nishikawa, D. Edelstein, X. Du, S. Yamagishi, T. Matsumura, Y. Kaneda, M.A. Yorek, D. Beebe, P.J. Oates, H.P. Hammes, I. Giardino, M. Brownlee, Normalizing mitochondrial superoxide production blocks three pathways of hyperglycaemic damage, Nature 404 (2000) 787–790.
[17] A. Morita, J. Zhu, N. Suzuki, A. Enomoto, Y. Matsumoto, M. Tomita, T. Suzuki, K. Ohtomo, Y. Hosoi, Sodium orthovanadate suppresses DNA damage-induced caspase activation and apoptosis by inactivating p53, Cell Death Differ. 13 (2006) 499–511.
[18] E. Appella, C.W. Anderson, Post-translational modifications and activation of p53 by genotoxic stresses, Eur. J. Biochem. 268 (2001) 2764–2772.
[19] X. Wu, Y. Deng, Bax and BH3-domain-only proteins in p53-mediated apoptosis, Front. Biosci. 7 (2002) d151–d156.
[20] G.A. Turenne, P. Paul, L. Laflair, B.D. Price, Activation of p53 transcriptional activity requires ATM's kinase domain and multiple N-terminal serine residues of p53, Oncogene 20 (2001) 5100–5110.

Please cite this article in press as: N. Sasano et al., Edaravone, a known free radical scavenger, enhances X-ray-induced apoptosis at low concentrations, Cancer Lett. (2010), doi:10.1016/j.canlet.2009.12.020